

GROWTH AND CHARACTERIZATION OF $(\text{In}_x\text{Ga}_{1-x})_2\text{O}_3$ THIN FILMS
GROWN BY PULSED LASER DEPOSITION

by

Sneha Karen Kawal, B.S.

A thesis submitted to the Graduate Council of
Texas State University in partial fulfillment
of the requirements for the degree of
Master of Science
with a Major in Engineering
August 2019

Committee Members:

Ravi Droopad, Chair

Qingkai Yu

William Stapleton

COPYRIGHT

by

Sneha Karen Kawal

2019

FAIR USE AND AUTHOR'S PERMISSION STATEMENT

Fair Use

This work is protected by the Copyright Laws of the United States (Public Law 94-553, section 107). Consistent with fair use as defined in the Copyright Laws, brief quotations from this material are allowed with proper acknowledgement. Use of this material for financial gain without the author's express written permission is not allowed.

Duplication Permission

As the copyright holder of this work I, Sneha Karen Kawal, authorize duplication of this work, in whole or in part, for educational or scholarly purposes only.

ACKNOWLEDGEMENTS

I would like to sincerely thank Dr. Ravi Droopad for giving me the opportunity to join his research group, for being my research advisor, and providing an excellent lab facility for me to conduct my research. His continuous guidance and valuable advice helped me throughout the course of the research.

I would also like to thank the members of Dr. Droopad's research group Shafiqur Rahman, Susmita Ghose, Juan Salvadore, Khem Baral, Brian Samuels and Dalim Mia for their help and assistance with various measurements and analysis.

In addition, I would like to thank my graduate advisor Dr. Vishu Visvanathan for his valuable advice and encouragement and the rest of my thesis committee, Dr. William Stapleton and Dr. Qingkai Yu for their support.

I would like to thank my family for always supporting and encouraging me.

TABLE OF CONTENTS

	Page
ACKNOWLEDGEMENTS.....	iv
LIST OF TABLES	vii
LIST OF FIGURES.....	viii
ABSTRACT.....	x
CHAPTER	
I INTRODUCTION	1
1.1 Literature Review.....	9
1.1.1 Crystal Structure of In_2O_3	9
1.1.2 Crystal Structure of Ga_2O_3	10
1.1.3 Material Properties of In_2O_3	12
1.1.4 Methods of growth of In_2O_3	13
1.1.5 Material properties of Ga_2O_3	17
1.1.6 Growth methods of Ga_2O_3	18
1.1.7 Alloy of $(\text{In}_x\text{Ga}_{1-x})_2\text{O}_3$	21
II GROWTH METHOD AND CHARACTERIZATION TECHNIQUES	25
2.1 Film Deposition Technique	25
2.1.1 Pulsed Laser Deposition.....	25
2.1.2 Target Preparation.....	26
2.2 Structural Characterization	27
2.2.1 X-ray Diffraction	27

2.3 Optical Characterization	28
2.3.1 Spectroscopic Ellipsometry.....	28
2.3.2 UV-Vis Spectroscopy	31
2.3.3 Atomic force Microscopy (AFM)	32
III. GROWTH AND CHARACTERIZATION OF $(\text{In}_x\text{Ga}_{1-x})_2\text{O}_3$ FILMS	34
3.1 Film Growth.....	34
3.1.1 Experimental	34
3.1.2 Results and Discussion	35
IV. CONCLUSION	49
REFERENCES.....	50

LIST OF TABLES

Table	Page
1. Material properties of important semiconductors and β -Ga ₂ O ₃	6
2. The lattice and positional parameters for different phases of In ₂ O ₃	10
3. Lattice parameters for polymorphs of Ga ₂ O ₃	11

LIST OF FIGURES

Figure	Page
1.1 Band diagram of GaAs/AlGaAs heterojunction-based HEMT, at equilibrium.	3
1.2 (a) Breakdown field as a function of bandgap, (b) theoretical limits of on-resistances vs. breakdown voltage plot for conventional semiconductors and β -Ga ₂ O ₃	8
1.3 Crystal structure of cubic bixbyite In ₂ O ₃ with the b and d sites	10
1.4 Depiction of the unit cell of β -Ga ₂ O ₃ along the c-(1), a-(2) and b-axis	12
1.5 Diagram of the atomic arrangement in In ₂ O ₃ (111) and Al ₂ O ₃ (0001)	17
1.6 Subsolidus phase diagram for Ga ₂ O ₃ -In ₂ O ₃ system	24
2.1 Schematic diagram of PLD system	26
2.2 Schematic diagram representing Bragg's law	28
2.3 Schematic diagram of ellipsometry	29
2.4 J.A. Woollam spectroscopic ellipsometry	30
2.5 Shimadzu UV-VIS-NIR optical spectrophotometer	31
2.6 The schematic diagram of AFM.....	32
2.7 Park XE7 AFM system.....	33
3.1 (a): XRD spectra of different (In _x Ga _{1-x}) ₂ O ₃ compositions grown at substrate temperature of 650°C and oxygen pressure of 10 ⁻² Torr.....	38
(b) FWHM values of different (In _x Ga _{1-x}) ₂ O ₃ compositions for (-603) plane	39

3.2 Peak position as a function of x.....	39
3.3 XRD spectra of $(\text{In}_x\text{Ga}_{1-x})_2\text{O}_3$ grown at various substrate temperatures at oxygen pressure of 10^{-2} Torr.....	40
3.4 (a) Spectroscopic Ellipsometry of a film of In content $x=0.2$ using Cauchy dispersion model; (b) n and k values	42
3.5 n and k (at $\lambda=632\text{nm}$) for $(\text{In}_x\text{Ga}_{1-x})_2\text{O}_3$ as a function of x	43
3.6 (a) Transmittance spectra (b) Tauc plot.....	44
(c) Optical bandgap as a function of x compared to values obtained by previous literature; for samples varying in In content grown at temperature of 650°C and oxygen pressure 10^{-2} Torr	45
3.7 Transmittance spectra for samples of In content $x=0.1$, grown at different temperature and oxygen pressure of 10^{-2} Torr.....	46
3.8 Atomic Force Microscopy (AFM) images of the films grown at a temperature of 650°C at different oxygen pressure	47
3.9 AFM images of samples grown at 650°C and 700°C, at an oxygen pressure of 10^{-3} Torr.....	48

ABSTRACT

Silicon has been an important material in the integrated circuit (IC) technology and is a commonly used elemental semiconductor. However, silicon has limitations in its operating voltage, temperature and switching frequency. Furthermore, being an indirect bandgap semiconductor, it is unsuitable for optoelectronic device applications. Wide bandgap semiconductors that include GaN and SiC is being used for power application but their breakdown field is limited. A new generation of power semiconductor devices based on materials having a larger breakdown field will help increase the efficiency of alternative electric energy transmission and generation. Due to its excellent thermal and chemical stability, beta-gallium oxide ($\beta\text{-Ga}_2\text{O}_3$) is a promising material for high breakdown, high-power devices. It's large direct bandgap of 4.9 eV is predicted to have a high breakdown electric field of 8 MV/cm for fabricated electronic devices. The large bandgap of $\beta\text{-Ga}_2\text{O}_3$ makes it transparent from the visible to UV wavelengths and can be alloyed with In_2O_3 to provide tunable bandgaps.

The growth of $(\text{In}_x\text{Ga}_{1-x})_2\text{O}_3$ with varying indium content (x) on sapphire (0001) substrates using pulsed laser deposition was demonstrated. X-ray diffraction (XRD) measurements revealed an increase in the lattice parameter as In content was increased as expected for an increase in lattice constant. The films were found to exhibit a predominantly monoclinic crystal structure for an In content $x=0.1$ grown at 650°C with a small amount of polycrystalline cubic structure present. As the indium content

increased from $x=0.1$ to $x=0.4$, the cubic structure of films became dominant. The optical constants (n , k) were determined using spectroscopic ellipsometry and found to vary with In content $x=0.1$ to 0.4 ranging between 1.8 to 2 for n while the k values range between 0.0002 to 0.0005 at a wavelength of 632 nm. The small value of k is expected since the bandgap of the material is large.

The percentage transmittance of the films is determined by ultraviolet visible spectroscopy with the films exhibiting large transmittance values in the visible region. The extracted bandgap was found to decrease with increase in indium content as expected.

I. INTRODUCTION

At the end of the 1940s, the era of modern semiconductors started with the arrival of pure single crystal germanium along with the breakthrough in understanding pn-junctions and the invention of the transistor.^[1] Ge was replaced by silicon in the 1950s and lost its importance for electronic devices. Ge has a small band gap of only 0.67 eV (at 300 K) which limited its operating temperature to $\sim 70^{\circ}\text{C}$. Silicon whose bandgap is 1.1 eV and has other properties that makes it suitable for most applications, has become the most commonly used semiconductor. It belongs to group IV elements in the periodic table and one of the major advantages of silicon is that it is inexpensive, mechanically strong and non-toxic, thus making it suitable for fabricating a variety of devices with good electrical properties. According to Moore's law, it is now possible to make high density miniature transistors on a single piece of silicon due to scaling. This increase in density has led to the present boom in information technology^[2]. The major scaling limiting factors for silicon device technology include leakage currents and intrinsic parameter fluctuations. The ultimate limitation of the scaling of transistors is the atomic structure of matter, thus a MOSFET cannot be smaller than an atom. However, one of the disadvantages of Si is that it has a relatively small bandgap and is only useful for devices that have small breakdown fields and as such is limited for high power and high-temperature applications. Another disadvantage of Si is being an indirect semiconductor and therefore its use in optoelectronic applications is limited. Other classes of direct bandgap materials that include the III-V system are ideal for efficient opto-electronic devices used for LEDs and lasers. Materials with a wider bandgap having a high breakdown voltage are more suitable than Si for power devices^{[3][4]}. These include SiC,

GaN and more recently Ga₂O₃ are being considered for high power high breakdown devices.

Gallium arsenide (GaAs) is a compound semiconductor of the III-V element group. Since GaAs allows high switching frequencies, it has gained significance for microwave devices. It has a bandgap of 1.4 eV and a room temperature electron mobility that is five times that of Si. ^[1] Because of its high electron mobility, it is suitable for high voltage Schottky diodes and high performance RF devices. It can be used as a substrate for other III-V semiconductors such as InGaAs. It is also used in High Electron Mobility Transistor (HEMT) structures. A HEMT is an important device in which there is a junction between two materials with different bandgaps. HEMTs are used for high speed, high frequency digital circuits^[5]. They are also used in high frequency products such as cell phones and satellite receivers. The advantage of a HEMT over a Si MOSFET is the higher electron mobility in GaAs compared with Si. For conduction, semiconductors are doped with impurities which donate either mobile electrons or holes. These impurities collide with the electrons and slow them down. High mobility electrons, that are generated at the heterojunction of a highly doped wide-bandgap n-type donor-supply layer and a non-doped narrow-bandgap channel layer with no dopant impurities, are used to overcome the drawback of low speed electrons. In figure 1.1, the depleted AlGaAs layer after the electrons have been completely dropped into the GaAs, is shown. In the conduction band on the GaAs side, a heterojunction is created by different bandgaps of the materials thus forming a quantum well. The electrons can move quickly without colliding with any impurities in the GaAs layer as it is undoped.

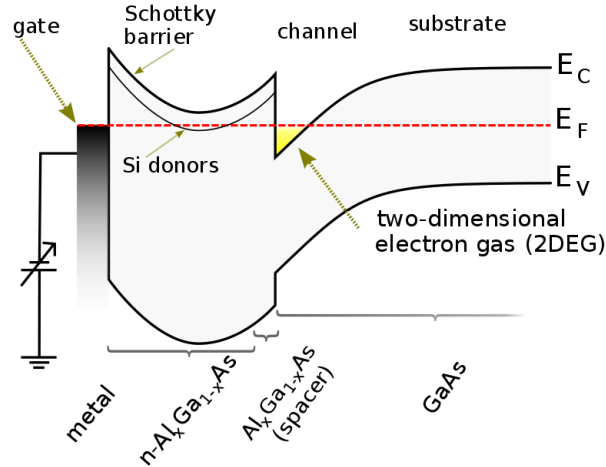


Figure 1.1: Band diagram of GaAs/AlGaAs heterojunction-based HEMT, at equilibrium^[6]

The disadvantage of GaAs is that it is a brittle material and has a low hole mobility compared to silicon which makes applications such as p-type MOS transistors not feasible. In addition, GaAs devices are expensive since they are difficult to fabricate.

Silicon carbide (SiC) has a large band gap ranging from 2.3 to 3.3 eV depending on the modification of the crystal (polytype).^[1] SiC has a much higher maximum operating temperature compared to Si. Because of its high critical field, fabrication of fast Schottky diodes and other unipolar devices for high voltages are possible. SiC devices are used in high blocking voltage and lower power loss pn-devices. SiC also provides for higher operation frequencies. Although the technology of SiC is less developed, it has a high potential. Schottky diodes and MOSFETs for currents up to 50 A and voltages up to 1700 V are being currently used.^[1]

Gallium Nitride (GaN) is another III-V group semiconductor which is widely used in microwave transistors that require high temperatures and power. GaN has a bandgap of 3.4 eV and a high critical field that is similar to 4H-SiC.^[1] However, GaN is difficult to dope to provide p-type regions. It is used in blue LEDs. Large single crystals

and wafers of GaN are difficult to fabricate and as such GaN films have been grown epitaxially on other substrates such as silicon, 4H-SiC or sapphire. GaN field-effect transistors (FETs) with blocking voltages up to 1.8 kV and currents of more than 100 A have been demonstrated. ^[1] High switching applications for voltages <1 kV have been developed. Special devices of the 600 V class are available in the market. Today, GaN substrates are used in UV or blue laser diodes, high brightness LEDs for general lighting and high power, high frequency transistors.

The properties of a semiconductor can be determined by its band structure and dopants added to it. Further insight into the properties of a semiconductor can be provided by a more detailed energy band representation in k-space ^[1]. The energy difference between the absolute minimum of the conduction band and the maximum of the valence band is the band gap E_g .^[1] The valence band maximum is nearly always at $k=0$. In GaAs, the minimum of the conduction band is also located at this position. This kind of semiconductor is called a direct semiconductor. For Si, the conduction band minimum is far away from $k=0$. This is an indirect semiconductor. The suitability of optical and power devices depends on whether a semiconductor is direct or indirect. When some atoms in the lattice of a silicon crystal are replaced by atoms of a group V element in the periodic table, each impurity atom has one electron more in the outer shell for the four covalent bonds. These elements donating the fifth electron to the conduction band are called donors. This is an extrinsic, n-type semiconductor with “n” pointing to the negative charge of the carriers. If the silicon atoms are replaced at some lattice points by atoms of a group III element, each impurity atom has one electron less than for the four covalent bonds. These impurities accepting an electron of the valence band and generating a mobile hole leading to p-type conductivity are called acceptors.

Semiconductors that enable devices to operate at much higher voltages, frequencies and temperatures than conventional semiconductor materials such as silicon and gallium arsenide are called wide bandgap semiconductors. Non-wide-bandgap materials including Si have a bandgap in the order of 1 to 1.5 electron volt (eV) while wide-bandgap materials typically have bandgaps ranging from 2 to 4 eV. Wide-bandgap devices are therefore able to operate at much higher temperatures, in the order of 300°C with high power. Wide-bandgap semiconductors (WBG), such as silicon carbide (SiC) and gallium nitride (GaN) can also reduce switching losses thereby increasing the efficiency and have the potential to operate in more harsh environments, higher voltages, and switching frequencies. Since wider bandgap materials have a high breakdown voltage, they are more suitable than Si for power devices ^{[3], [4]}. By reducing the size of passives and cooling systems, WBG semiconductors can provide smaller, lighter, and less expensive power conversion equipment. Direct wide-bandgap materials also find applications in ultraviolet electronics including emitters and detectors. Being expensive, high-quality SiC and GaN substrates are not favorable for mass production of power devices. Therefore, new materials are required to overcome this limitation.^[7] Devices based on wide-bandgap materials can increase the efficiency of alternative electric energy transmission and generation.^[8]

Gallium oxide (Ga_2O_3) is a new oxide semiconductor compound whose bandgap is ~4.9 eV, which is larger than both GaN and SiC.^[9] Ga_2O_3 has five different crystal structures which are α , β , γ , δ and ϵ phase. β - Ga_2O_3 is the most stable form both thermally and chemically among all phases. It has deep-ultraviolet transparent conductive property. β - Ga_2O_3 is highly stable since its crystal structure is base centered monoclinic in which the oxygen ions are in a distorted cubic packing arrangement whereas the

gallium ions are in distorted tetrahedral and octahedral sites. For β -Ga₂O₃, n-type doping is the most popular technology with Sn and Si identified as donors that have small activation energies. Wide range of electron densities (n) of 10^{15} - 10^{19} cm⁻³ is caused by controlled doping ^{[10][11]}. Because of the wide bandgap of Ga₂O₃, hole conduction in Ga₂O₃ has not been reported so far. Due to a very limited hole mobility, a very small effective p-type conductivity was predicted in Ga₂O₃ ^[12]. Ga₂O₃ is also used as a transparent conducting oxide (TCO) layer. TCOs are electrically conductive materials whose absorption of light in the visible region of the electromagnetic spectrum is comparably low. Thin film technologies are usually used to prepare TCOs which can be used in optoelectronic devices such as solar cells and displays. Due to their great electro-optical properties, TCOs have a great potential and make promising candidates for light modulation or active plasmonics.^[13] A comparison on important properties of materials between major semiconductors and β -Ga₂O₃ is shown in Table 1.

Table 1: Material properties of important semiconductors and β -Ga₂O₃ ^[14]

	Si	GaAs	4H-SiC	GaN	Diamond	β -Ga ₂ O ₃
Bandgap, E_g (eV)	1.1	1.4	3.3	3.4	5.5	~4.9
Electron mobility, μ (cm ² V ⁻¹ S ⁻¹)	1400	8000	1000	1200	2000	300
Breakdown field, E_b (MVcm ⁻¹)	0.3	0.4	2.5	3.3	10	8
Relative dielectric constant, ϵ	11.8	12.9	9.7	9.0	5.5	10
Baliga's FOM, $\epsilon\mu E_b^3$	1	15	340	870	24664	3444
Thermal conductivity (Wcm ⁻¹ K ⁻¹)	1.5	0.55	2.7	2.1	10	0.23 [010] 0.13 [100]

In Table 1, it is seen that β -Ga₂O₃ has a bandgap of ~4.9 eV which is larger than Si, GaAs, 4H-SiC and GaN making it a promising candidate for numerous applications since it is highly transparent from the visible to UV wavelengths.^{[3][14]} Most of the transparent conductive oxides such as In₂O₃, SnO₂, ZnO and ITO are useful for numerous applications but their small band gaps (~3eV) make them unsuitable for opto-electronic devices operating in the UV wavelength region^[15] The breakdown field of a material refers to the voltage at which a device can operate, beyond this voltage breakdown occurs. The breakdown field of β -Ga₂O₃ is predicted to be approximately 8 MV/cm, which is three times larger than those of 4H-SiC and GaN.^[16] Because of its high breakdown electric field, higher thermal stability and intrinsic solar blindness have been demonstrated^[3] The Baliga's FOM of β -Ga₂O₃ is at least four times larger than those of 4H-SiC or GaN. The Baliga figure of merit (FOM) indicates the suitability of a material for a power device. BFOM corresponds to the lowest specific on-resistance of a vertical electronic device which makes β -Ga₂O₃ an excellent candidate for low loss, high-voltage switching applications such as high-breakdown Schottky diodes and field-effect transistors^[16].

The breakdown electric field of important materials as a function of their bandgap is shown in figure 1.2 (a). The estimated breakdown electric field for Ga₂O₃ is 8 MV/cm, from interpolation between bandgaps and breakdown electric field. Because of the high breakdown electric field, β -Ga₂O₃ is a promising candidate in the high-power electronics field. Figure 1.2 (b) shows a plot of the theoretical limits of on-resistances vs. breakdown voltage calculated from the given parameters in Table 1 for well-known materials. Since β -Ga₂O₃ devices have a high breakdown voltage, it exhibits lower on-resistance, and hence lower conduction loss compared to Si, SiC, and GaN devices.^[16]

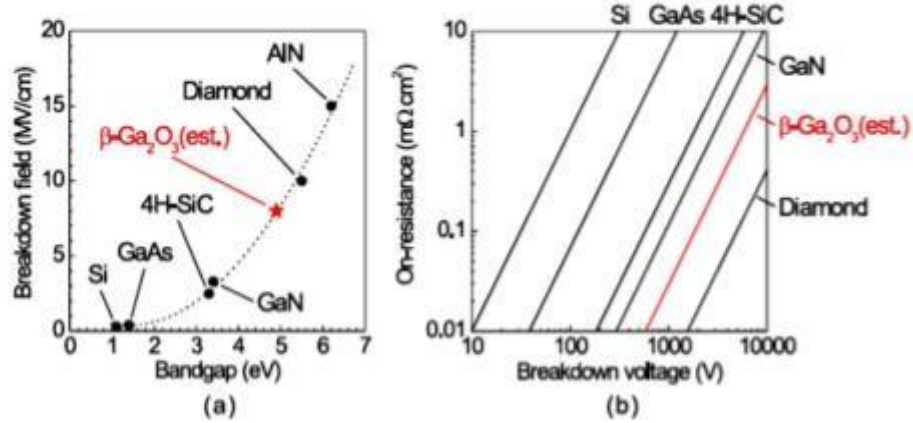


Figure 1.2: (a) Breakdown field as a function of bandgap, (b) theoretical limits of on-resistances vs. breakdown voltage plot for conventional semiconductors and $\beta\text{-Ga}_2\text{O}_3$.^[16]

Indium oxide (In_2O_3) is an n-type semiconductor which has a wide bandgap in the range of 3.5 to 4 eV^[17]. The oxygen vacancies in this oxide material act as donors in In_2O_3 ^[17]. In_2O_3 exists in three polymorphs namely cubic bixbyite, rhombohedral corundum-type and orthorhombic referred to as c- In_2O_3 , rh- In_2O_3 and o- In_2O_3 respectively. These polymorphs have been studied using soft x-ray absorption spectroscopy (XAS) and soft x-ray emission spectroscopy (XES) in previous research^[18]. The crystalline structure for many indium oxide based TCOs is that of bixbyite structure.^[19] It is a structure in which one-quarter of the anions are missing thus producing structural vacancies. In this structure, the oxygen atoms are octahedrally coordinated around indium. All indium cations are surrounded by six oxygen atoms and two structural vacancies. In_2O_3 finds application in solar cells, light-emitting diodes and liquid-crystal displays^[18].

In this study, In_2O_3 is alloyed with Ga_2O_3 to enable tuning of the bandgap in the range 3.5-4.9 eV which will enable potential applications including wavelength-tunable optoelectronic devices and high electron mobility transistors (HEMTs)^[20]. The growth

and properties of the indium gallium oxide alloys are discussed. The objective of this thesis is to study the growth and properties of the thin films of indium gallium oxide alloys for In composition ≤ 0.4 .

1.1 Literature Review and Properties of wide bandgap oxides

1.1.1 Crystal Structure of In_2O_3

Indium oxide (In_2O_3) is an ionically bonded semiconducting oxide. It crystallizes into a cubic bixbyite-type structure with a space group $Ia\bar{3}$ and its lattice parameter that measures 10.118 nm. There are 80 atoms contained in the unit cell of indium oxide. At two types of non-equivalent six-fold coordinated sites, 32 sites are occupied by cations. These two different six-fold coordinated sites are called “b” and “d” sites, according to international notation. One quarter of the cations are found on trigonally compressed octahedral “b” sites and the remaining three-quarters of the cations are found on the highly distorted octahedral “d” sites. On both “b” and “d” sites, indium atoms occupy the center of a distorted cube. Oxygen atoms are positioned at six corners of this cube while the remaining two corners remain unoccupied. For the “b” sites, oxygen vacancies occur along the body diagonal whereas for the “d” sites they are located along a face diagonal. A schematic representation of the crystal structure of In_2O_3 with the b and d sites is shown in figure 1.3.

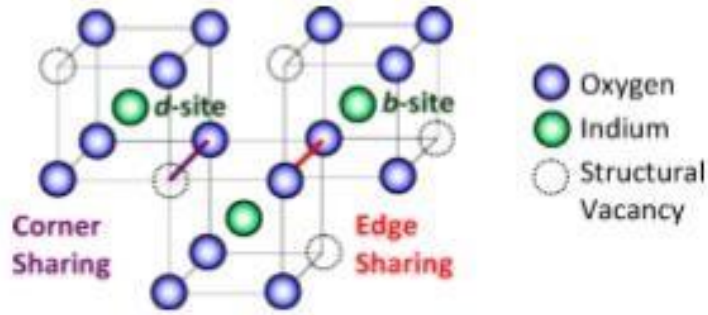


Figure 1.3: Crystal structure of cubic bixbyite In_2O_3 with the b and d sites.^[19]

The lattice and positional parameters for different phases of In_2O_3 were calculated as given in table 2 below:^[18]

Table 2: The lattice and positional parameters for different phases of In_2O_3

Compound and space group	Unit cell (Å)	Wyckoff				
		Atom	site	x	y	z
c- In_2O_3	$a = 10.1170$	In1	8b	0.25000	0.25000	0.25000
$Ia\bar{3}$	$a = 10.1170$	In2	24d	0.46650	0.000	0.25000
	$a = 10.1170$	O	48e	0.39085	0.15435	0.38140
rh- In_2O_3	$a = b = 5.4814$	In	12c	0.0000	0.000	0.35720
$R\bar{3}c$	$c = 14.4998$	O	18e	0.96367	0.33333	0.58330
o- In_2O_3	$a = 7.9295$	In	8d	0.11483	0.74607	0.02627
Pbcn	$b = 5.4821$	O1	8d	0.85114	0.61188	0.09552
	$c = 5.55898$	O2	4c	0.0000	0.03792	0.25000

1.1.2 Crystal structure of Ga_2O_3

The β -form of gallium oxide is the most common amongst its polymorphs. The remaining polymorphs of gallium oxide are metastable and at temperatures above 750900 centigrade become β - Ga_2O_3 . These polymorphs differ in their crystal space group as well

as the coordination number of Ga ions present. A description of gallium oxide's polymorphs which are designated α , β , γ , δ and ϵ can be seen in Table 3:

Table 3: Lattice parameters for polymorphs of Ga_2O_3 (adapted) ^[9]

Polymorph	Structure	Space group	Lattice parameters
α	rhombohedral	$R3c^-$	$a = 4.9825 \text{ \AA}$ $c = 13.433 \text{ \AA}$
β	monoclinic	$C2/m$	$a = 12.23 \text{ \AA}$ $b = 3.04 \text{ \AA}$ $c = 5.80 \text{ \AA}$ $\beta = 103.7^\circ$
γ	cubic	$Fd3m^-$	$a = 8.238 \text{ \AA}$
δ	bodycentered cubic	$Ia3^-$	$a = 10.00 \text{ \AA}$
ϵ	orthorhombic	$Pna2_1$	$a = 5.120 \text{ \AA}$ $b = 8.792 \text{ \AA}$ $c = 9.410 \text{ \AA}$

The latest and most accurate study of the crystal structure of β - Ga_2O_3 was published by Ahman et al. ^[21] The results slightly differ from the previously published data of Konh and Geller ^[22] but are much more precise. X-ray diffraction symmetry clearly indicated a c-centered monoclinic cell with space group $C2/m$. The unit cell of β - Ga_2O_3 is shown in figure 1.4. Two crystallographically inequivalent Ga positions exist: Ga (I) which has a tetrahedral geometry, and Ga (II) which has an octahedral geometry. The oxygen ions are arranged in a distorted cubic close-packed array. There are three different crystallographical positions for an oxygen atom which are denoted as O(I), O(II),

and O(III). One oxygen atom is coordinated tetrahedrally while the others are coordinated trigonally.

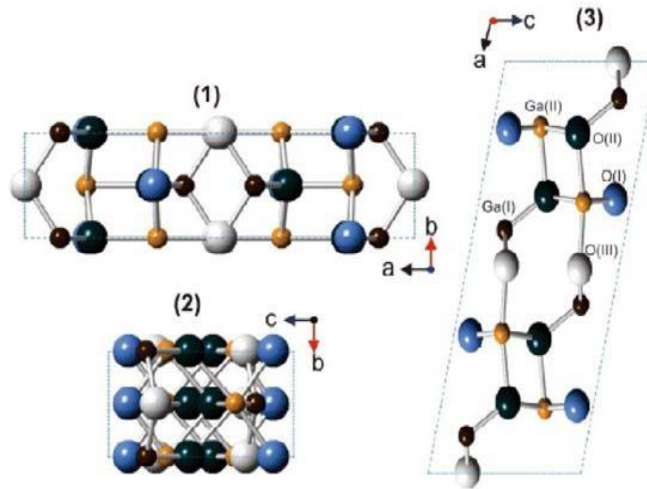


Figure 1.4: Depiction of the unit cell of β - Ga_2O_3 along the c-(1), a-(2) and b-axis^[23]

In its monoclinic phase, Ga_2O_3 holds useful critical properties for high-power devices with large electrical breakdown and its alloy indium gallium oxide broadens its application to encompass tunable bandgap devices in the ultraviolet spectrum.

1.1.3 Material Properties of In_2O_3

Indium oxide is a wide band-gap semiconductor (energy gap $E_g \sim 3.70 \text{ eV}$ ^[24]). It acts as an insulator in the stoichiometric form (In_2O_3). If prepared in its oxygen deficient form (InO_x) it can reach high n-type doping levels ^[25]. Indium oxide is a transparent conducting oxide with a high conductivity when not intentionally doped (free carriers up to 10^{17} – 10^{19} cm^{-3} range) ^[26]. When doped, usually with 9% tin oxide, it becomes indium tin oxide (ITO) which is one of the most popular transparent conducting electrodes used in thin-film photovoltaics and flat-panel display devices. ITO has a high transparency for visible light (85% at wavelengths from 340 to 780 nm) combined with the lowest

electrical resistivity ($7.7 \times 10^{-5} \Omega \text{ cm}$)^[28]. In one research by Subramani Shanmugan *et al.*^[28], it was found that the transmittance spectra of O₂ plasma-processed indium oxide films had lower transmittance between 8% and 18%. Films processed at low plasma power with a high O flow rate showed very low transmittance less than 10%. This low optical transmittance was attributed to insufficient availability of oxygen. The unoxidized indium acts as scattering centers for light, hence the low optical transmittance at lower oxygen partial pressures. The higher transmittance (~18%) observed in the films was attributed to less scattering effects, structural homogeneity and better crystallinity, whereas, the lower transmittance (~8%) might be on account of less crystallinity leading to more light scattering^[29]. Also, having a moderately lower transparency could be explained by the existence of donor levels as a result of oxygen vacancies^[30].

1.1.4 Methods of growth of In₂O₃

In₂O₃ films can be fabricated by various methods including sputtering^[28], spray pyrolysis^[31], chemical-vapor deposition (CVD)^[32], molecular-beam epitaxy (MBE), and pulsed laser deposition (PLD)^[33].

Indium thin films were deposited by RF Magnetron Sputtering on soda lime glass substrates in an atmosphere of Ar at ambient temperatures^[28]. Pure In (99.999%) was used as the sputtering target while high pure argon gas was used as the working gas. The base pressure of the chamber was $\sim 2 \times 10^{-7}$ Torr. A gas flow rate of 14 sccm and a gas pressure of 1.4×10^{-2} Torr were used during the deposition with an RF power of 40 W. Adjustments were made to the duration of sputtering to produce In films of thicknesses of about 100 nm. Deposition rate for coating of the In films was 0.09 nm/sec. Oxygen plasma with a plasma power of 100 W and 200 W, gas flow rate of 15 and 20

sccm and process time 5 and 10 mins were used for the sputtered films. The XRD results showed that the samples had peaks that corresponded to the rhombohedral structure of In_2O_3 films with (110) orientation. A lower transmittance between 8% and 18% was observed in the transmittance spectra for all the films. The films that were processed at low plasma power with high O_2 flow rate showed low transmittance $<10\%$. The low optical transmittance was suggested to be due to insufficient oxygen available. The higher transmittance ($\sim 18\%$) observed was attributed to less scattering and better crystallinity while the lower transmittance ($\sim 8\%$) was attributed to more scattering and less crystallinity. The absorption coefficient was in the range between 7.5×10^4 and $1.25 \times 10^5 \text{ cm}^{-1}$. It was observed that the absorption coefficient decreased with the increase of wavelength and oxygen partial pressure. The band gap was observed to decrease with increase in plasma power and oxygen gas flow rate.

Indium oxide thin films were prepared by the method of spray pyrolysis in which pure indium chloride powder (99.99%) and deionized water were mixed up to 40 mL solution with molarity of 0.1 M as solvent^[31]. The samples were deposited at spray rate of 2 mL/min, 3.5 mL/min, and 5 mL/min. The samples were then annealed at 500°C for 1 hour in air atmosphere. XRD analysis revealed that the films were of polycrystalline cubic structure. A trend was observed in the variation of the structural properties in the samples before and after annealing. A high transparency ($\sim 70\%$) was observed in the optical characterization of the films. Increased oxygen vacancies caused the bandgap of the samples to decrease after annealing.

In another research, indium oxide nano crystals were synthesized by direct oxidation of In with oxygen and incorporation of ammonium chloride in the indium under nitrogen^[32]. NH₃ was used to yield In nano crystals. The limitation of the synthesis of In₂O₃ nano crystals by direct oxidation of In with O₂ by the formation of an oxide shell surrounding the indium could be eliminated only at a growth temperature > 900°C. The XRD spectra revealed that the In₂O₃ nano crystals grown at 1000°C on silicon (111) had a cubic structure. The reflection spectrum revealed the optical bandgap to be nearly 3.5 eV.

In another research by R.K. Gupta *et al.*^[33], high quality thin films were grown on a quartz substrate by pulsed laser deposition in which a sintered ceramic In₂O₃ target with a purity of 99.999 was used at substrate temperatures varying from room temperature to 600°C (under vacuum of base pressure 1.2×10^{-9} bar) and under oxygen pressures of 5.0×10^{-7} bar, 1.0×10^{-6} bar, 2.5×10^{-6} bar, 6.0×10^{-6} bar, and 1.0×10^{-5} bar (at substrate temperature of 400°C). The main chamber was initially evacuated to 1.2×10^{-9} bar and during deposition, oxygen gas was introduced into the chamber to obtain the pressures mentioned above. The thickness of the films was approximately 100 nm. The laser pulse rate was 10 Hz, laser operating energy was 300 mJ/pulse.

There was a 45° angle of incidence between the laser beam and the rotating target. For an increase in the crystallinity of the films, low oxygen pressure in the PLD chamber was favored during the growth. Higher transmittance (~90%), lower electrical resistivity (1.7×10^{-4} Ω.cm), and higher mobility ($119 \text{ cm}^2\text{V}^{-1}\text{s}^{-1}$) were observed in the characterization of films grown. It was observed that the transmittance of the films was affected by the growth temperature. The films grown at room temperature had the least optical

transparency. The optical transparency increased with increase in the growth temperature. The average percentage transmittance of the films grown at room temperature, 200°C, 400°C, and 600°C were 55%, 72%, 77%, and 89%, respectively. The films grown in an oxygen atmosphere had an improved transparency compared to those grown under vacuum at the same substrate temperature. The average percentage optical transparency for the films grown under oxygen atmosphere at room temperature, 200°C, 400°C and 600°C were found to be 66%, 83%, 89% and 90% respectively. It was also observed that the films grown at 200°C had the least resistivity compared to the films grown at other temperatures. Further, the films grown at 200°C had the highest carrier concentration, which decreased with the increase in growth temperature accompanied with an increase in the mobility. It was observed that the mobility increased from 32 to 98 $\text{cm}^2\text{V}^{-1}\text{s}^{-1}$ as the growth temperature increased from room temperature to 600°C. The XRD spectra of In_2O_3 films revealed that the crystallinity in the deposited films depended on the growth temperature. The effect of oxygen pressure on the crystallinity of the films grown at 400°C were studied. It was observed that low oxygen pressure during the growth of the films favored the formation of films with improved crystallinity. The XRD spectra revealed the single-phase body-centered cubic crystalline indium oxide structure. Raman spectra for indium oxide films also showed the presence of cubic phase. AFM results showed that the growth temperature had an effect on the film morphology. The film grown at 200°C in vacuum was smoother compared to films grown at 600°C. The presence of oxygen during the growth of the films also had an effect on the surface morphology of the films. The films grown under an oxygen pressure of 1×10^{-6} bar (750×10^{-6} torr) at 400°C were observed to have the least surface roughness.

Mei *et al.* studied In_2O_3 grown on sapphire (0001) substrates by MBE to determine the relationship between the orientations of In_2O_3 (111) and Al_2O_3 (0001) [34]. It was observed that the hexagonally packed indium plane of In_2O_3 (111) was matched parallelly to the closely-packed oxygen plane of sapphire (0001) with a 30° rotation from the main lattice. Also, the parallel orientations of In_2O_3 ($11\bar{2}$) and sapphire ($11\bar{2}$) using high-resolution electron microscopy (HREM) was shown. The atomic arrangement of In_2O_3 (111) and Al_2O_3 (0001) are shown in figure 1.5.

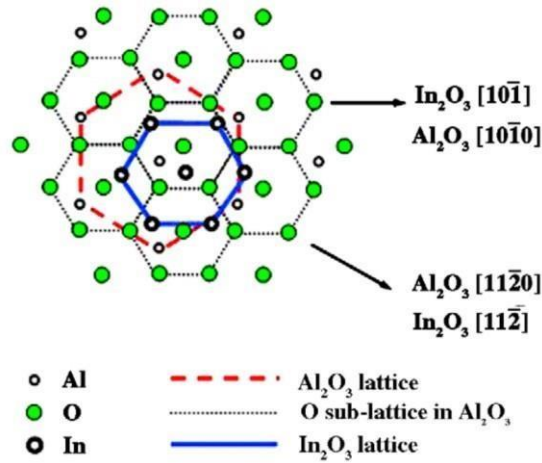


Figure 1.5: Diagram of the atomic arrangement in In_2O_3 (111) and Al_2O_3 (0001) [34]

1.1.5 Material properties of Ga_2O_3

Ga_2O_3 has a bandgap of approximately 4.9 eV, which is larger than the bandgaps of GaN and SiC which are 3.4 eV and 2.3-3.3 eV respectively. It can be crystallized in five different structures: α , β , γ , δ and ϵ phases. Thermally and chemically, β - Ga_2O_3 is the most stable form. Its crystal structure is base-centered monoclinic in which the oxygen ions are in a distorted cubic packing arrangement and the gallium ions are in distorted tetrahedral and octahedral sites. Ga_2O_3 is used as a Transparent Conducting Oxide (TCO) and is used in solar-blind photoconductors as UV detectors.

1.1.6 Growth methods of Ga₂O₃

In a research conducted by Susmita Ghose *et al.* [35], β -Ga₂O₃ thin films were grown by MBE using a Ga₂O₃ compound source and an elemental Ga source, with oxygen plasma in the latter case. With the use of the compound source, no additional oxygen was necessary to grow β -Ga₂O₃ as oxidized Ga and oxygen from the source were present. The required oxygen needed to form Ga₂O₃ was obtained from the decomposition of the polycrystalline Ga₂O₃ source and transported to the surface of the substrate along with the Ga₂O molecules. In plasma assisted MBE (PAMBE) technique, growth of β -Ga₂O₃ was carried out in an oxide MBE chamber with a base pressure of $< 5 \times 10^{-10}$ Torr using a combination of turbomolecular and cryopumps. The oxygen was supplied from a RF plasma source with a DC bias on the deflector plate to reduce the ions from reaching the substrate. RHEED was used to monitor the growth. The thin films were deposited on single-side polished quarter of 2" c-plane sapphire substrates. The substrate temperatures were varied from 650-750°C. The oxygen gas flow rate was 1.24 sccm and the input RF plasma power was 300 W. When the growth temperature was increased from 650-750°C, the XRD spectra showed four diffraction peaks corresponding to the (-201),(-402),(-603) and (-804) planes of β Ga₂O₃. A pure single phase (-201) oriented β -Ga₂O₃ was seen. The AFM images revealed the root mean square (RMS) surface roughness of the films grown using elemental Ga source with growth temperatures of 650, 700 and 750°C as 0.37,1.11 and 0.39 nm respectively.

In a research conducted by Kohei Sasaki *et al.* [36], β -Ga₂O₃ thin films were grown directly on Si-doped n-type and Mg-doped semi-insulating substrates by MBE. Ga and Sn were evaporated from 6 N Ga metal and 4 N SnO₂ powder that was heated in normal

K-cells. The oxygen source was a mixture of 5% ozone and 95% oxygen. It was not possible to grow Ga₂O₃ when 100% oxygen gas was used, since almost all of the supplied oxygen molecules had re-evaporated. Hence ozone was used as the oxidizing power of ozone is stronger than oxygen. The substrate temperature was 600, 700 or 800°C. The Ga beam equivalent pressure (BEP) was 3×10^{-5} or 2×10^{-4} Pa. The ozone-oxygen gas mixture flow rate was 1 or 5 sccm. The growth time was 1 or 2 hours. The reflection high-energy electron diffraction (RHEED) was used to analyze the crystal quality of the films. The RHEED pattern of the epitaxial films had a sharp streak line which was similar to the substrate after polishing, thereby revealing homoepitaxial film formation. Atomic Force Microscopy (AFM) and Nomarski microscopy was used to study the surface morphology of the films. AFM images showed a roughness of 0.7 nm.

In a research conducted by L.X Qian^[37], two sapphire substrates were cleaned in acetone, methanol and de-ionized water for 5 min each. One of the substrates was subjected to annealing at 760°C in the plasma-assisted MBE chamber under a vacuum of 6.6×10^{-6} Pa (0.0495×10^{-6} Torr). Next, a 100-nm thick β -Ga₂O₃ film was grown in-situ, during which Ga was evaporated from a Knudsen cell under 940°C while oxygen plasma was generated from a radio-frequency (RF) radical cell with an input power of 300 W. The substrates were heated at 760°C during the epitaxial growth. For the as-supplied sapphire substrate, the epitaxial growth of β -Ga₂O₃ thin film was conducted under the same conditions. The XRD spectra of β -Ga₂O₃ epitaxial films grown on the as-supplied and annealed sapphire substrates showed that there were three clear peaks belonging to β -Ga₂O₃ planes (-201), (-402) and (-603) except those belonging to sapphire substrate that indicated nearly single-crystal (-201) oriented growths on both substrates. The XRD

rocking curves of (-201) diffraction peak for the samples in which β -Ga₂O₃ thin films was grown on as-supplied and annealed sapphire substrates, revealed that the full width at half maximum (FWHM) values at (-201) plane were 1.9 ° and 1.0° respectively. It was observed that the intensity of (-201) diffraction peak for the β -Ga₂O₃ epitaxial film became significantly larger for the sample with annealed sapphire substrate. It was observed that the crystal quality improved substantially by using annealed sapphire substrate that could be explained by the effect of high-temperature-reconstructed sapphire surface on the adsorption, clustering and crystallization of molecules. The AFM result revealed a large number of protrusions that were distributed uniformly on the surface of the annealed sapphire substrate proving an effective high-temperature reconstruction by the treatment. In conclusion, this work demonstrated how the pre-treatment of the sapphire substrate in high vacuum by MBE makes it effective to fabricate β -Ga₂O₃ solar-blind DUV photodetector.

In a research conducted by P. Marie ^[38], gallium oxide thin films were prepared by means of radio-frequency (rf) magnetron sputtering of a gallium oxide target with a purity of 99.9% at temperatures between 100–600°C on single crystal silicon substrates under argon pressure of 2.5×10^{-2} Torr and power density of 2.5 W/cm². The thickness of the films ranged between 250 nm and 600 nm. For each substrate temperature, (100)-oriented silicon substrates were placed in the chamber, alongside each other 7cm above the target. Post-annealing temperatures were 900°C and 1000°C for 1 hour under the continuous flow of pure nitrogen. The β -Ga₂O₃ phase was visible upon an anneal treatment at about 900°C. The intensity was observed to be high for the (400) plane thus indicating a (400) orientation of the films. The sample annealed at 1000°C had a more

intensified β -Ga₂O₃ phase. A better figure of merit up to 1.9×10^{-4} was achieved at the annealing temperature of 1000 °C.

1.1.7 Alloy of (In_xGa_{1-x})₂O₃

Bandgap engineering is significant for device applications in heterostructures. Heterostructures consist of two materials with different bandgaps. The alloy of (InGa)₂O₃ is a promising material for semiconductor devices due to the large bandgap range of 3.7 – 4.9 eV covering the wavelength range of 253 – 335 nm. This wavelength range falls within the ultraviolet (UV) spectrum enabling the use of the alloy in UV opto-electronic devices, photodetectors and high electron mobility transistors (HEMTs). β -Ga₂O₃ based high power HEMTs are promising due to the large bandgap that leads to an expected high electric breakdown voltage. The reason for using In and Ga to make the alloy is that both belong to the same column III element group and have the same electronic structure. The expected crystal structure of the alloy depends on the of fabrication conditions. Since In₂O₃ and Ga₂O₃ have different crystal structures that are cubic and monoclinic respectively, phase separation between the two crystal structures is expected depending on the In content. (InGa)₂O₃ can be used as transparent conducting oxide (TCO). Its absorption coefficient is low in the visible range thereby making it suitable for applications such as coatings on transparent substrates including plastic, glass and semiconductors^{[39][40]}. This alloy can be grown by various methods such as MBE and PLD.

Work presented by Zhang *et al.* has demonstrated (InGa)₂O₃ film growth on sapphire (0001) at substrate temperature of 500 °C by PLD over a variety of compositions^[20]. For indium content between 0.16 and 0.33, mixed phases of the cubic

and monoclinic structures was observed. With an indium content of less than 0.16, only the monoclinic phase was seen. An indium content above 0.83 revealed the single crystal cubic structures while for indium content between 0.33 – 0.56, polycrystalline cubic structure with XRD peaks representing the (222) and (400) orientations was revealed. The optical transmission spectra was measured indicating bandgap increasing from 3.8 eV to 5.1 eV corresponding to the increase in gallium content from 0 to 100 % respectively.

In a study by Oshima and Fujita, the phase separation between cubic In_2O_3 and monoclinic Ga_2O_3 using MBE was examined^[41]. The samples were grown on double-polished c-plane sapphire (0001) substrates at 800 °C and Ga beam equivalent pressure (BEP) of 1.1×10^{-7} Torr with a buffer layer of monoclinic Ga_2O_3 . XRD scans revealed the cubic structure at an indium composition of 43% but due to the buffer layer it was unclear at which indium composition the film became entirely single crystal cubic. They observed a degradation in crystallinity for high indium composition. It was also suggested that low temperature growth was necessary to minimize the phase separation. The transmission spectra revealed that the transmittance of all films exceeded 85% and the bandgap calculated ranged between 5.0 eV and 4.0 eV, with the increase in In composition up to 35%. They suggested that these films could be used in wavelength-tunable photodetectors.

In a research by Z Zhang^[42], thin films of $(\text{In}_x\text{Ga}_{1-x})_2\text{O}_3$ were grown by PLD on a 2 inch diameter, double-sided polished c-plane sapphire wafer. The In_2O_3 and Ga_2O_3 targets were prepared by ball milling, pressing and sintering for 12h at 1600°C and 72h at 1350°C, respectively. The ceramic targets were cut into halves and a target was obtained from one semicircular In_2O_3 and one semicircular Ga_2O_3 target. The growth temperature

was about 650°C while the oxygen background pressure was 10^{-5} mbar. XRD spectra revealed that for low In content ($x < 0.15$), the thin film had monoclinic crystal structure while for highest In contents ($x > 0.8$), the cubic bixbyite phase was observed. For the intermediate alloys, the rhombohedral $\text{InGaO}_3(\text{II})$ crystallographic phase was observed. Transmittance spectra revealed that the optical bandgap decreased from 4.9 eV to 4.5 eV with increasing indium content from $x=0.006$ to $x=0.15$. The bandgap had a linear dependency on the In content x for parts of the sample having the monoclinic phase, only. The bandgap was found to be approximately 3.5 eV for the cubic phase (indium content $x > 0.8$) while the bandgap was found to be 3.7 eV for the rhombohedral phase, (indium content $x=0.65$).

In a research by Fabi Zhang and Qixin Guo ^[43], $(\text{GaIn})_2\text{O}_3$ films were prepared by pulsed laser deposition on (0001) sapphire substrates at room temperature (RT). The films were grown with an oxygen pressure of 0.1 Pa (0.00075 Torr), laser energy of 225 mJ, frequency of 1Hz and a deposition rate of 40 minutes. The indium content in the target were 0.2, 0.3, 0.5 and 0.7. The films maintained the (-201) oriented monoclinic structure of $(\text{GaIn})_2\text{O}_3$ up to a nominal indium composition of 0.3 while the films with nominal indium content of 0.5 and 0.7 show cubic structured (222) oriented diffraction patterns. Moreover, it was observed that with increasing nominal indium content, both the (-402) peak position of monoclinic and (222) peak position of cubic structures of $(\text{GaIn})_2\text{O}_3$ films shifted gradually toward a lower angle suggesting an increase in the lattice constant. The co-existence of double structures had not been observed clearly.

In a previous research conducted by Doreen D Edwards and group ^[44], the phase relationships in the $\text{Ga}_2\text{O}_3\text{-In}_2\text{O}_3$ system were studied by X-ray diffraction and electron

probe microanalysis (EPMA) for the temperature range of 800-1400°C. It was noted that the solubility limit of In₂O₃ in the β-gallia structure decreased with increasing temperature from 44.1 ± 0.5 mol% at 1000°C to 41.4 ± 0.5 mol% at 1400°C while the solubility limit of Ga₂O₃ in cubic In₂O₃ increases with temperature from 4.0 ± 0.5 mol% at 1000°C to 10.0 ± 0.5 mol% at 1400°C. The phase diagram for Ga₂O₃-In₂O₃ system is shown in figure 1.6.

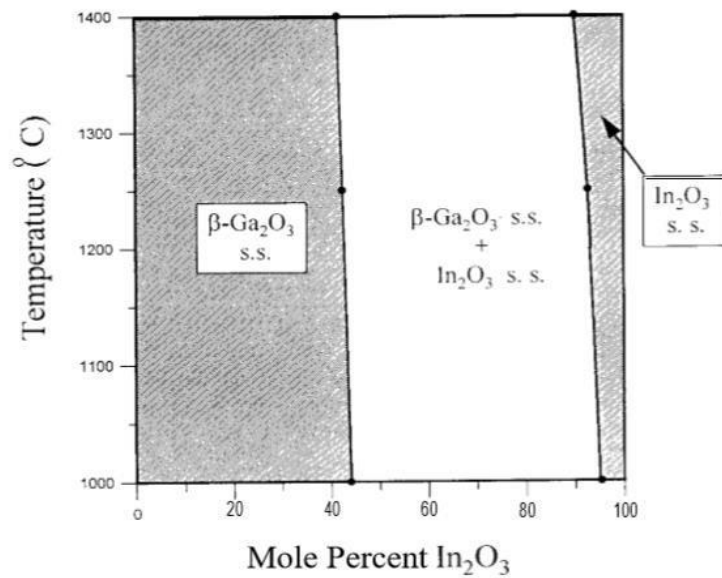


Figure 1.6: Subsolidus phase diagram for Ga₂O₃-In₂O₃ system

In this study, thin films of (InGa)₂O₃ alloy with indium composition ranging between 10% to 40% will be grown to investigate their crystal structure and optical properties. The effects on the films by growth temperature and oxygen pressure used during growth will also be studied.

II. GROWTH METHOD AND CHARACTERIZATION TECHNIQUES

2.1 Film Deposition Technique

2.1.1 Pulsed Laser Deposition

Pulsed laser deposition (PLD) is a simple technique to deposit thin films. It has several advantages over other deposition techniques. The film growth rate can be controlled by PLD with the help of a laser system. ^[7] Stoichiometry of target and the film can be maintained. Multilayered films can be produced by different materials using PLD. The contamination of films can also be minimized in PLD since the laser beam is focused on the source material during deposition. PLD technique is carried out in ultrahigh vacuum with the laser placed outside the vacuum chamber. The target material in the vacuum chamber is vaporized by the high power laser and is deposited as a thin film on the substrate. ^[45] A transfer arm is used to transfer the substrate and target into the growth chamber from the load lock chamber. The substrate holder and target holders are located within the main chamber. The temperature of the substrate during deposition can be controlled with the help of a radiative heater that is contained within the substrate holder. A turbomolecular pump controls the chamber pressure. A base pressure of $\sim 10^{-9}$ Torr can be obtained with the pump and the pressure can be varied by partially closing the gate valve. The laser interacts with the target through a transparent port. The target and the substrate are rotated to ensure uniform deposition of the thin films. ^[46] During growth, the laser strikes the surface of the target and excites the species on it which can be seen as a 'plume' that expands in the direction perpendicular to the target. The excited species start to form a film on the surface of the substrate that is placed within the trajectory of

this plume. ^[47] The laser that is used to ablate the material from the target is a COMPEX Pro KrF excimer laser with a wavelength of 248 nm. Energy density (fluence), pulse duration, wavelength and laser repetition rate are the various laser parameters that play a role in the formation of the film^[7]. The schematic diagram of a typical PLD chamber is shown in figure 2.1. ^[47]

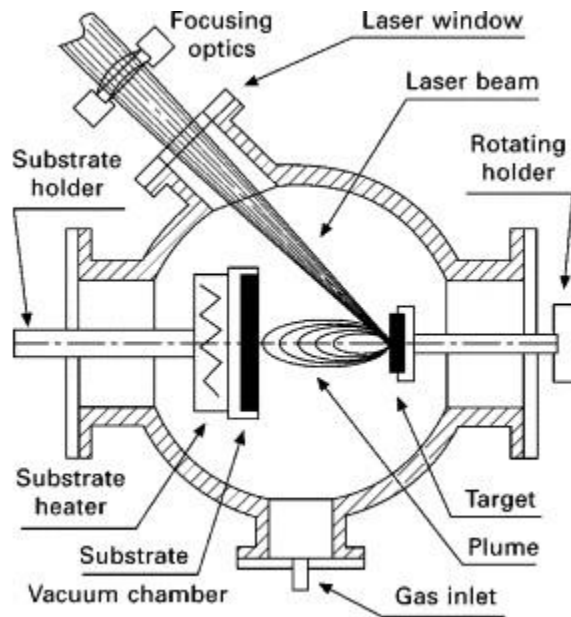


Figure 2.1: Schematic diagram of PLD system ^[47]

2.1.2 Target Preparation

For deposition of films by the PLD technique, a dense target is prepared to ensure longer working life of the target and to avoid cracking or over-heating of the target. The targets undergo a solid state process known as “ceramic sintering”, in which heat is used to transform a powder into a solid, dense ceramic. The powder is a combination of high purity oxide powders in the desired atomic ratio. A ball miller is used to mix the powders for an hour to ensure uniform distribution throughout the target. The mixture is then placed into a mold and pressed at a pressure of approximately 19000 lb/in² and

temperature of 450°C for a period of 20 hours using a heated hydraulic press. The ceramic target is further sintered in a tube furnace at a temperature of 1000°C in argon gas for 20 hours. The dense target is then placed into the main chamber of the PLD system for growth of thin films.

2.2 Structural Characterization

2.2.1 X-ray Diffraction

X-ray diffraction (XRD) is a phenomenon in which x-ray photons are scattered by atoms in a periodic lattice. These scattered monochromatic x-rays that are in phase give constructive interference ^[48] Figure 2.2 illustrates how x-ray diffraction by crystal planes allows one to derive lattice spacings by using the Bragg's law $n\lambda = 2d \sin \theta$, where n is an integer called the order of diffraction, λ is the wavelength of x-rays, d is the spacing between the crystal planes and θ is the angle between the incident beam and the normal to the reflecting lattice plane. By measuring the angle θ , the interplanar spacings, d , of every single crystallographic phase can be determined. XRD spectra can reveal properties of the material such as its crystal structure, crystalline quality, orientation, as well as internal stress. By analyzing the peak positions and intensities in an x-ray diffraction pattern, the lattice constant can be determined.

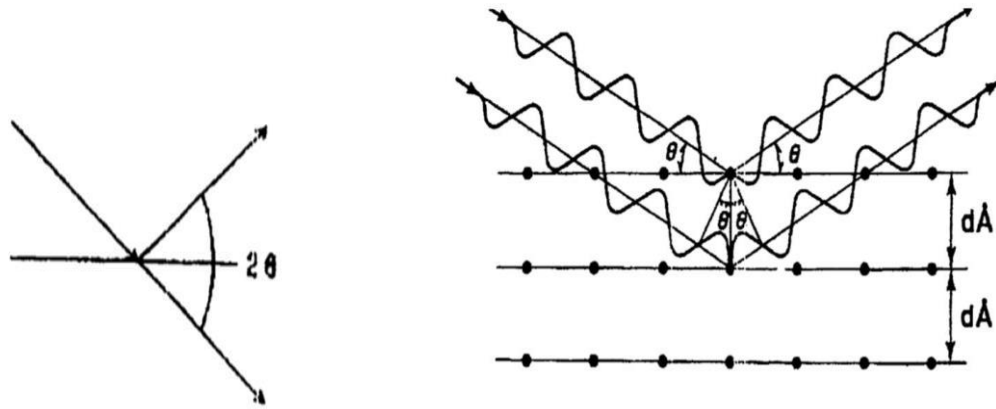


Figure 2.2: Schematic diagram representing Bragg's law. [48]

The diffracted rays are measured for intensity typically plotted versus 2θ where θ is the incident angle of the X-ray beam as illustrated in figure 2.2. The resulting spectrum is then compared to the database of known crystalline materials and analyzed to identify the orientation within the material.

2.3 Optical Characterization

2.3.1 Spectroscopic Ellipsometry

Spectroscopic ellipsometry provides information about the thin films grown such as their composition, thickness and roughness. The change in the polarization of light reflected from the sample surface is measured by taking the amplitude ratio of two perpendicularly polarized beams which is the principle of ellipsometry. The angle of incidence can be varied. [49] The schematic representation of an ellipsometer is shown in figure 2.3.

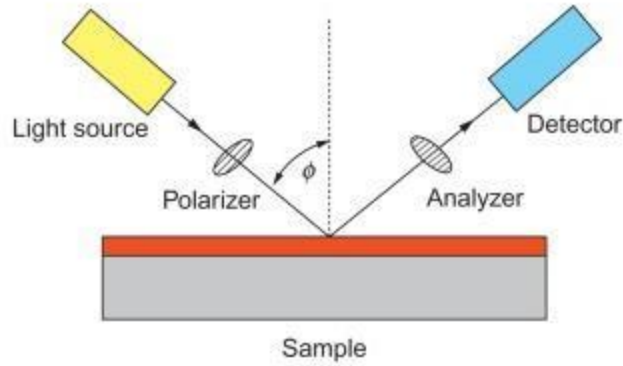


Figure 2.3: Schematic diagram of ellipsometry ^[49]

Linearly polarized light at angles of incidence that are non-normal becomes polarized elliptically on reflection from the material with asymmetric intensity difference ($\tan(\Psi)$ and phase difference (Δ)^[6]. These values are measured using ellipsometry and they are related to r_p and r_s , polarized components of the reflected amplitudes as shown below:

$$\rho = \tan(\psi)\exp(i\Delta) = r_p / r_s$$

where r_p and r_s are the amplitude reflection coefficients for the parallel and perpendicular components respectively ^[50]. The above ratio is called the complex Fresnel ratio. To determine the thickness and optical constants of the films, a model must be developed and fitted to ψ and Δ over a range of wavelengths. For dielectric function modelling in a transparent region, the Cauchy (or Cauchy absorbent) model is commonly used, and optical constants $n(\lambda)$ and $k(\lambda)$ are defined by:

$$n(\lambda) = A + \frac{B \times 10^4}{\lambda^2} + \frac{C \times 10^9}{\lambda^4}$$

$$k(\lambda) = D \times 10^{-5} + \frac{E \times 10^4}{\lambda^2} + \frac{F \times 10^9}{\lambda^4}$$

where A, B, C, D, E and F are fitting parameters and λ is the wavelength. The fitting of the experimental data (Ψ_{Exp} and Δ_{Exp}) to the modelled outputs (Ψ_{Theory} and Δ_{Theory}) is done by minimizing the mean-square error (MSE) χ^2 defined as:

$$\chi^2 = \frac{1}{2n - m - 1} \sum_{i=0}^n [(\tan \Psi_{Theory}^i - \tan \Psi_{Exp}^i)^2 + (\cos \Delta_{Theory}^i - \cos \Delta_{Exp}^i)^2]$$

where n is the number of Ψ/Δ pairs and m is the number of free parameters. The lowest value of χ^2 is taken as the correct model output. [7] Measurements were carried out using J.A Woollam spectroscopic ellipsometry shown in figure 2.4.

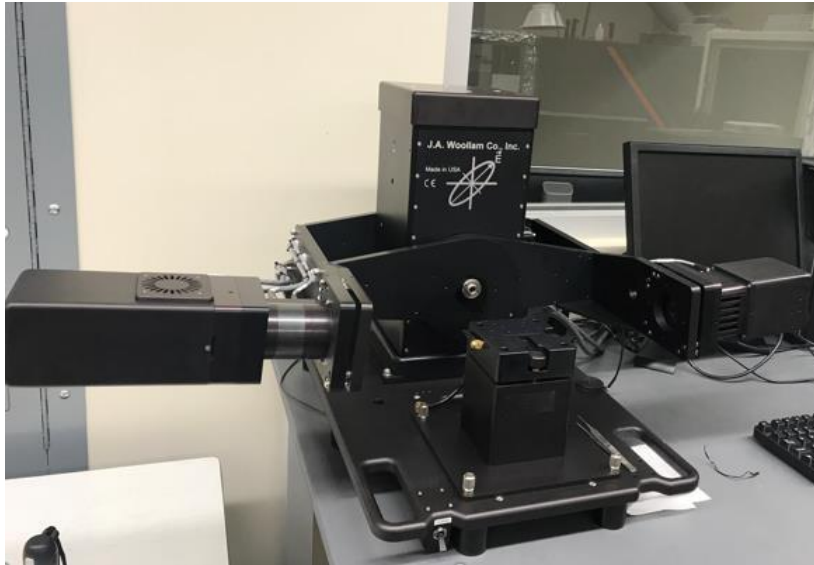


Figure 2.4: J.A. Woollam spectroscopic ellipsometry at Texas State University.

2.3.2 UV-Vis Spectroscopy

Ultraviolet-visible (UV-Vis) spectroscopy is a technique used to measure the absorption or transmittance of the electromagnetic spectrum in the ultraviolet to visible to near infrared wavelengths. In this method, a pair of emitters and detectors are used for a wavelength range between 200-900 nm. One emitter/detector pair passes light through the sample while the other pair passes light through a reference substrate, or through air. In this study, a sapphire substrate is used as the reference substrate for the measurements. The transmittance of the films is then obtained. From the transmittance data collected from the measurements, the bandgap can be calculated. Absorption of the film and the optical bandgap are related as follow:

$$(\alpha hv)^{1/2} = B(hv - E_g)$$

Where, α = absorption coefficient, B is the absorption edge width parameter, $h\nu$ is the photon energy, and E_g is the optical bandgap ^[51]. The measurements were carried out using Shimadzu UV-VIS-NIR optical spectrophotometer shown in figure 2.5.



Figure 2.5 : Shimadzu UV-VIS-NIR optical spectrophotometer at Texas State University.

2.3.3 Atomic force Microscopy (AFM)

AFM is a high resolution scanning technique in which a fine tip is used to probe the surface of a material. The advantage of AFM over other scanning techniques is that its resolution depends on the dimension of the tip and hence its resolution is higher compared to an optical microscope. The AFM scan shows the position of the tip. There are three imaging modes in AFM namely contact mode, non-contact mode and intermittent contact or tapping mode. In contact mode, a constant bend in the cantilever is maintained during scanning while in non-contact mode, the cantilever oscillates just above the specimen. The separation between the tip and specimen and the oscillation amplitude are in the order of 1 nm to 10 nm. AFM is generally used to analyze the morphology or topography for both conducting and insulating sample surfaces [52]. AFM is used to determine the roughness of deposited films. The schematic diagram of an AFM is shown in figure 2.6 [53] showing the sample stage, photo detector, laser diode and cantilever with sharp tip.

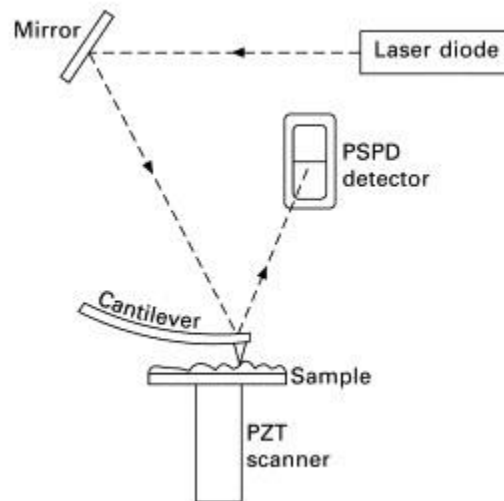


Figure 2.6: The schematic diagram of AFM

The sharp AFM tip which scans the sample surface is attached to the end of the cantilever. The cantilever deviates towards or away from the sample surface depending on attractive or repulsive forces experienced from the surface atoms. The working principle of AFM is based on the atomic attraction and repulsive force mapping between the atoms of the AFM tip and sample surface ^{[54][55]}. The AFM technique uses the Van der Waals force during scanning when the probing tip is very close to the sample surface and causes vertical deflection of cantilever. The measurement of the cantilever deflection requires a very sensitive technique due to the small force between sample and probe. The deflection signals can be transformed into surface morphology using a feedback electric current ^{[56][57]}. In this study, the AFM measurements of the thin films were carried out using Park XE7 Atomic Force Microscope shown in figure 2.7.

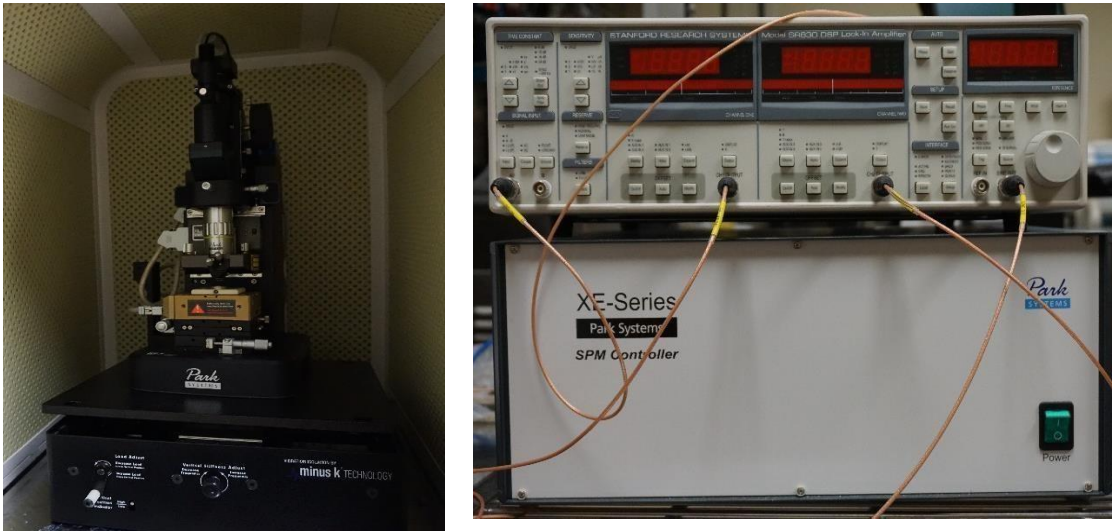


Figure 2.7 : Park XE7 AFM system at Texas State University

III. GROWTH AND CHARACTERIZATION OF $(\text{In}_x\text{Ga}_{1-x})_2\text{O}_3$ FILMS

3.1 Film Growth

3.1.1 *Experimental*

For the growth of films using the PLD technique, dense targets need to be fabricated. High purity (99.999 %) oxide powders are used to prepare the targets. The powders have different indium content with the molar ratios of $\text{In}/(\text{In} + \text{Ga})$ equaling 0.1, 0.2, 0.3 and 0.4. During growth of $(\text{In}_x\text{Ga}_{1-x})_2\text{O}_3$ films, the pressure of the chamber is set to $\sim 10^{-2}$ Torr with the introduction of oxygen and using a turbomolecular pump with a reduced speed of 170 Hz. The substrates used are two-inch diameter single-side polished c-plane sapphire wafers that are prepared by ultrasonically cleaning with organic solvents (acetone, isopropanol) followed by a deionized water rinse and dried with nitrogen gas. The target is loaded into the chamber from the load lock using a magnetic transfer arm. The substrate is heated to a fixed temperature for the particular deposition and placed at a distance of 5 cm above the target. Both the substrate and target undergo rotation during the growth process to ensure uniformity in the film thickness. A KrF excimer laser ($\lambda = 248$ nm) was used as the energy source with the energy set to 300 mJ at a pulse rate of 10 Hz. All films were grown for 20 mins. Deposition process takes place in the presence of oxygen gas. The film was then subjected to annealing for 30 mins after the deposition. After post-growth annealing, the substrate is cooled down and unloaded from the chamber once the temperature reaches 300°C . In this study, the films are grown with varying growth parameters that include temperature and the oxygen pressure in the chamber. The XRD measurements is used to analyze the crystal structure of the films grown.

By keeping the other growth parameters constant, films are grown at varying substrate temperatures of 400°C, 600°C, 650°C and 700°C to study the effect of the growth temperature on the films' crystalline quality, optical properties and surface morphology.

A set of films of the same composition were grown by varying the oxygen pressure at 10^1 Torr and 10^{-4} Torr while keeping other growth parameters such as laser parameters and growth temperature constant (at 650°C). The films were then studied for their crystalline quality, surface morphology and optical properties as a function of oxygen pressure during growth. It is expected that the roughness of the films will be reduced with lower oxygen pressure during growth because of the decrease in grain size at lower pressure.

3.1.2 Results and Discussion

XRD diffraction was used to investigate the crystalline properties of the grown films. A series of films were grown at a substrate temperature of 650°C and an oxygen pressure of 10^{-2} torr for different In composition. The rocking curve XRD measurements were performed on each thin film sample. The two theta-omega (2θ - ω) XRD scan of $(\text{In}_x\text{Ga}_{1-x})_2\text{O}_3$ thin films grown on sapphire is shown in figure 3.1 (a) for various indium content (x). The XRD spectra revealed four diffraction peaks other than peaks corresponding to the sapphire substrate for the film with In content $x=0.1$. These diffraction peaks correspond to (-201), (-402), (-603) and (-804) plane of the monoclinic structure of $(\text{In}_x\text{Ga}_{1-x})_2\text{O}_3$. A small peak corresponding to (222) plane (at $2\theta=30.9^\circ$) of the cubic bixbyite structure of $(\text{In}_x\text{Ga}_{1-x})_2\text{O}_3$ was also detected in the XRD pattern. At intermediate In content $x=0.2$ and $x=0.3$, the films exhibited both monoclinic and cubic

bixbyite structure. The peak intensities reduced for the monoclinic phase relative to the cubic phase with increase in the Indium content.

As the In content was varied from $x=0.1$ to $x=0.4$, the $(\text{In}_x\text{Ga}_{1-x})_2\text{O}_3$ alloy slowly transitioned into an almost cubic structure exhibited by peaks of high intensity corresponding to planes of cubic crystal structure. This phase transitioning of the films is in agreement with previous research by Zhang et al. ^[20] who demonstrated $(\text{InGa})_2\text{O}_3$ film growth on sapphire (0001) at 500°C by PLD over a variety of compositions. It was shown that for indium content between 0.16 and 0.33, mixed phases of the cubic and monoclinic structures were produced. With an indium content less than 0.16, only the monoclinic phase appeared in the XRD pattern. An indium content above 0.83 produced the single crystal cubic structures. For indium content between 0.33 – 0.56, polycrystalline cubic structure with XRD peaks representing the (222) and (400) orientations were present.

The XRD spectra obtained for the films grown in this study is supported by previous research by Oshima and Fujita ^[41], in which the phase separation between cubic In_2O_3 and monoclinic Ga_2O_3 using MBE was examined. All samples were grown on sapphire (0001) with a buffer layer of monoclinic Ga_2O_3 of thickness 10 nm, at various growth temperatures $>600^\circ\text{C}$ with controlled oxygen. The buffer layer was expected to suppress the phase separation. However, XRD scans revealed the appearance of cubic In_2O_3 at an indium composition of 43%, but due to the buffer layer it was unclear as to at which indium composition the film became entirely single crystal cubic. They also observed a degradation in crystallinity for high indium composition and low temperature growth was necessary to suppress the phase separation. It was observed that both

monoclinic and cubic phases occurred at indium content greater than 43%. The XRD data obtained in this research is in accordance with research stated above because mixed phases were observed for indium content of 40% even though the growth process was different. In this study, mixed phases were obtained at a lower In content $x=0.1$ compared to the previous researches conducted by Zhang *et al.* [20] and Oshima and Fujita [41] where mixed phases were obtained between In content $x= 0.16$ and 0.33 and above 43% respectively. This might be due to the difference in growth parameters in the growth methods. It could be due to the difference in substrate temperatures used to grow the films. Zhang *et al.* grew the films at a substrate temperature of 500°C while Oshima and Fujita grew the films at a temperature of 800°C . In this study, films of varying In content (x) were grown at 650°C . Substrate temperature plays an important role in the growth of the films. Higher the substrate temperature, greater is the thermal energy available for the adatoms to migrate on the surface. If the substrate temperature is low, the ad-atoms will not have adequate thermal energy to migrate on the surface and the nucleation will be reduced leading to a degradation in the crystallinity in the film.

The full width at half maximum (FWHM) values were calculated from the XRD data obtained as shown in figure 3.1 (b). It was clearly observed that with increase in In content from $x=0.1$ to $x=0.4$, the (-603) peak shifted towards a lower angle indicating an increase in lattice constant. This can be explained by the higher ionic radius of In^{3+} (0.81 \AA) compared to Ga^{3+} (0.62 \AA). As a result, with increase in In content, more In^{3+} ions entered into the lattice of Ga_2O_3 , thereby increasing the value of the lattice constant [38]. Lower FWHM values at lower In content indicated higher degree of crystallinity.

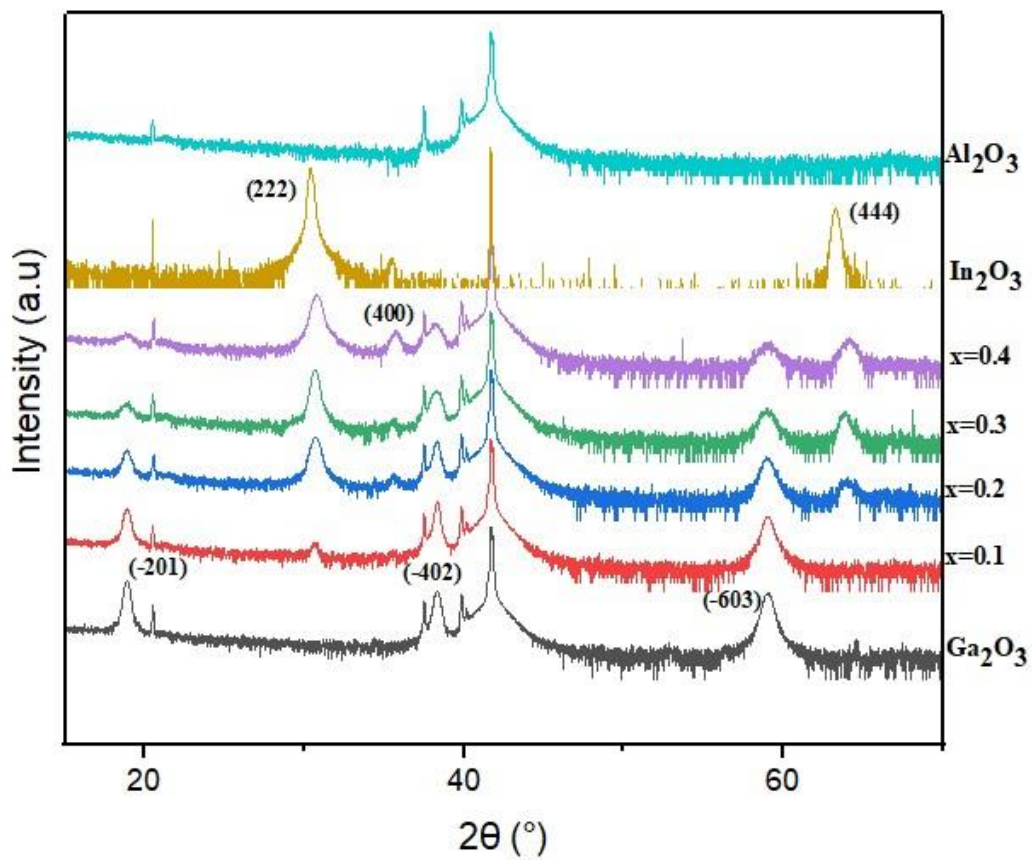


Figure 3.1 (a): XRD spectra of different $(\text{In}_x\text{Ga}_{1-x})_2\text{O}_3$ compositions grown at substrate temperature of 650°C and oxygen pressure of 10^{-2} Torr.

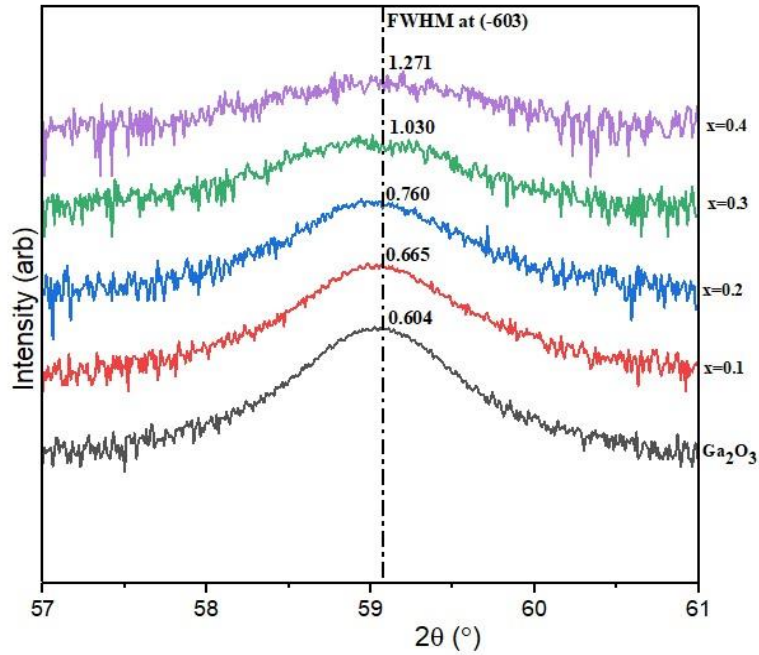


Figure 3.1 (b) FWHM values of different $(\text{In}_x\text{Ga}_{1-x})_2\text{O}_3$ compositions for (-603) plane .

The shift in peak position as a function of the In content x is shown in figure 3.2.

It can be clearly seen that the peak is gradually shifting towards a lower angle.

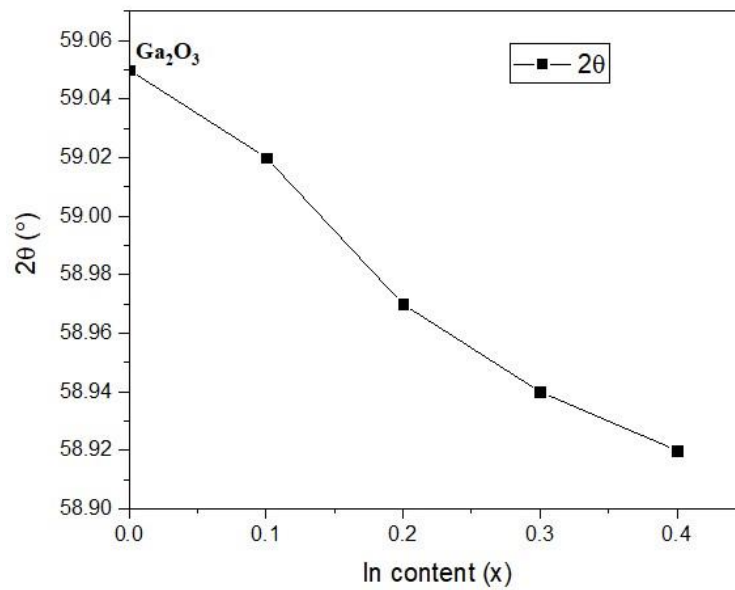


Figure 3.2: Peak position as a function of x

Further XRD measurements were taken for samples grown at different substrate temperatures under the presence of same oxygen pressure as can be seen in figure 3.3. The substrate temperatures were 400°C, 600°C, 650°C and 700°C. The oxygen pressure during growth was 10^{-2} Torr. The XRD spectra revealed the decline in the intensity of the peaks at (-603) plane as the temperature reduced from 700°C to 400°C. This decrease in intensity can be explained by the affect of substrate temperature on the films. At low substrate temperatures, the films exhibited degraded crystallinity, as can be seen by the reduction in peak intensities, since there is insufficient energy for the ad-atoms to migrate on the surface. When the substrate temperature was increased above 400°C, the crystallinity of the film increased due to the increased thermal energy for the ad-atoms to migrate.

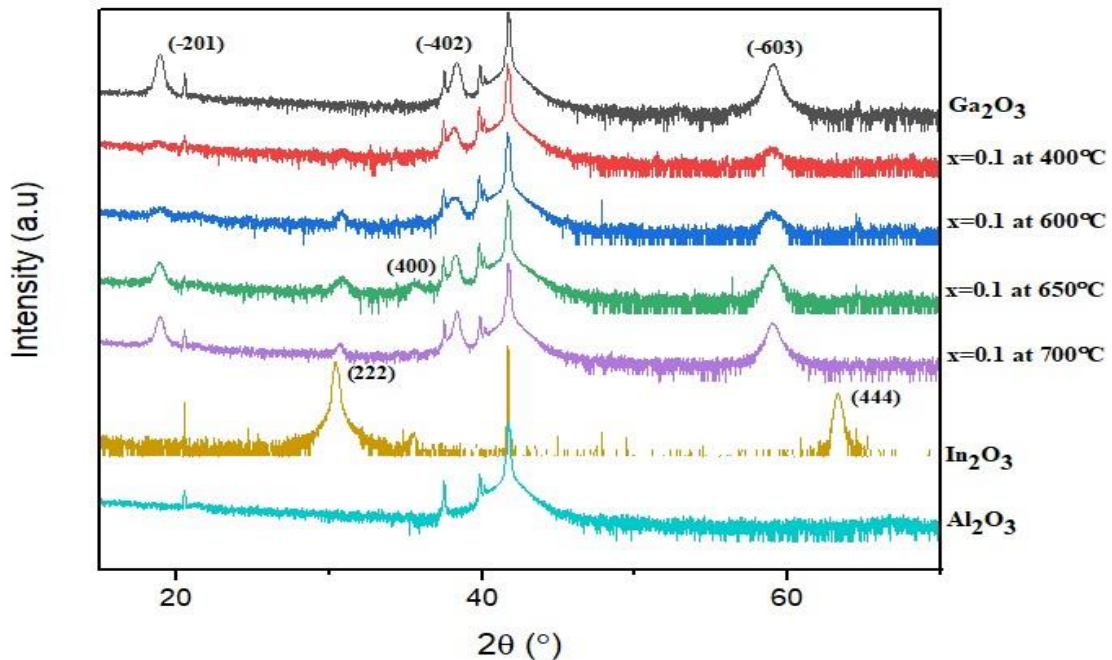
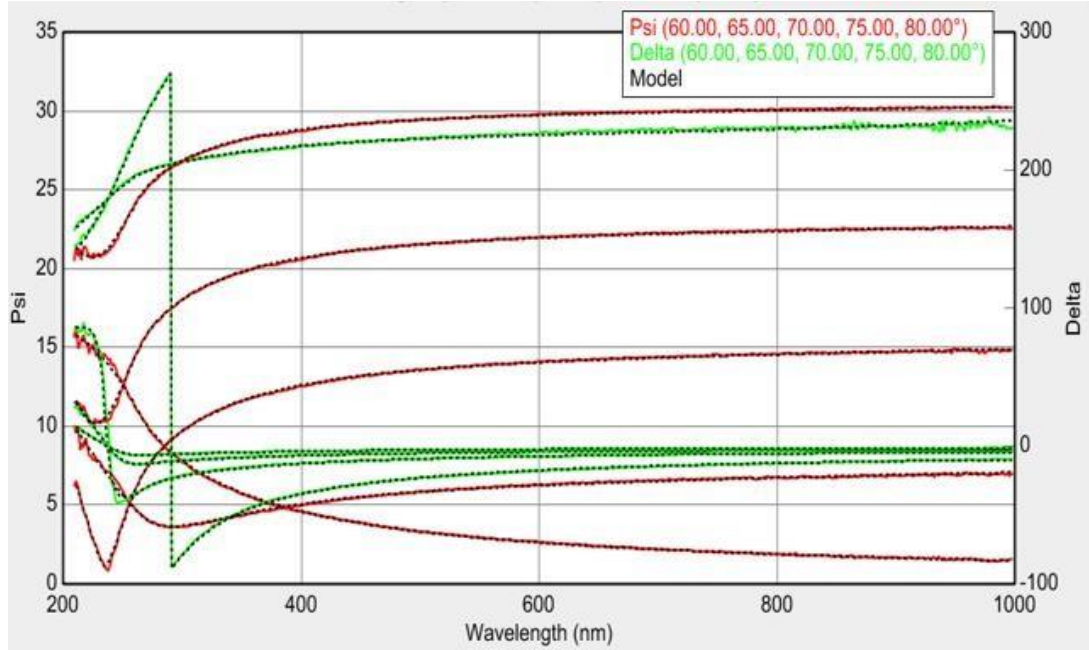


Figure 3.3: XRD spectra of $(\text{In}_x\text{Ga}_{1-x})_2\text{O}_3$ grown at various substrate temperatures at oxygen pressure of 10^{-2} Torr

Spectroscopic ellipsometry measurements were taken for samples varying in In content (x) in order to study the effects of composition on their optical properties. The ψ and Δ values obtained for a sample with In content $x=0.2$ grown under at 650°C and under an oxygen pressure of 10^{-2} Torr along with the Cauchy model used to fit the data is shown in figure 3.4 (a). The refractive index (n) and extinction coefficient (k) values were extracted from the model and displayed as a function of wavelength shown in figure 3.4 (b). The roughness and thickness of the film were also extracted from the ellipsometry model. The roughness for the film with In content $x=0.2$ was found to be ~ 1 nm while its thickness was ~ 24.5 nm. The n and k values for films is shown as a function of varying In content x in figure 3.5. The n and k values (at a wavelength of 632 nm) obtained for films varying in In content $x=0.1$ to 0.4 are ranged between 1.8 to 2 while the k values range between 0.0002 to 0.0005. The small value of k is expected since the bandgap of the material is large.

(a)



b)

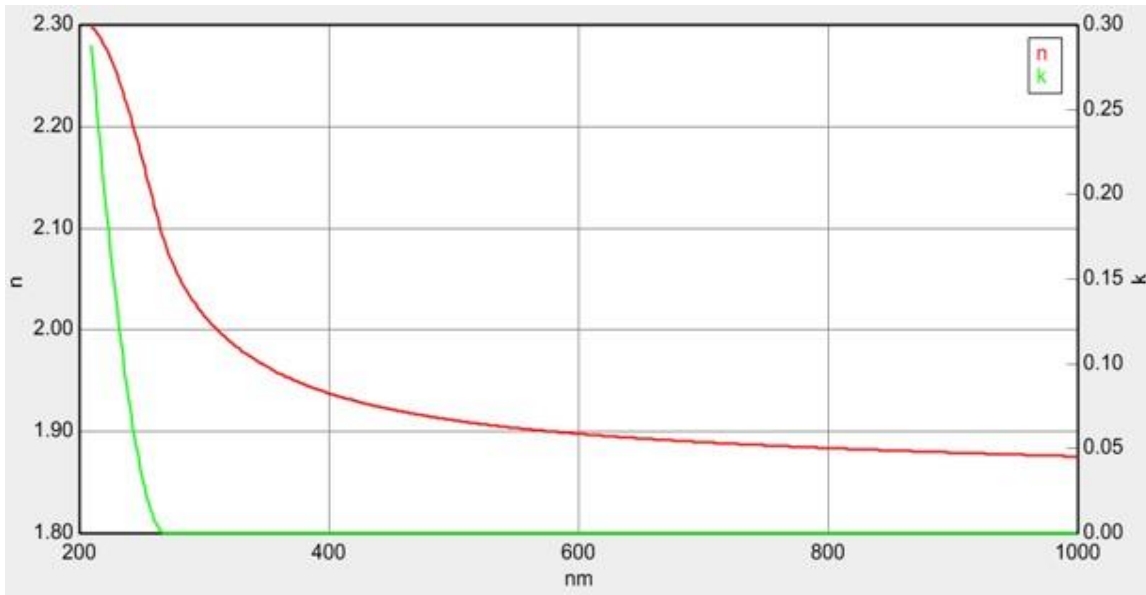


Figure 3.4 : (a) Spectroscopic Ellipsometry of a film of In content $x=0.2$ using Cauchy dispersion model;

(b) n and k values

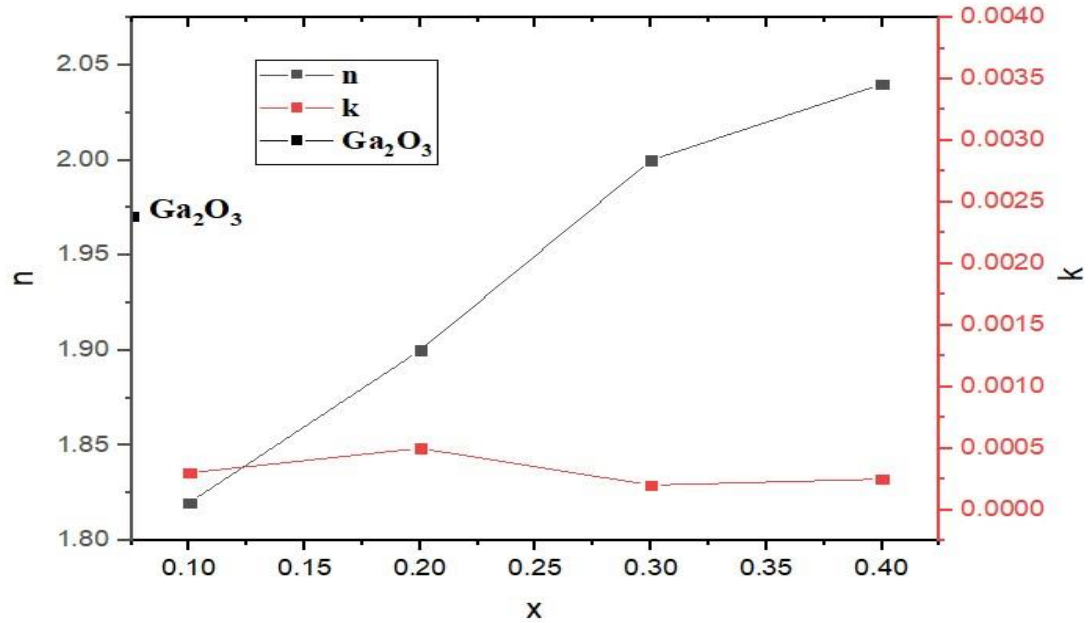
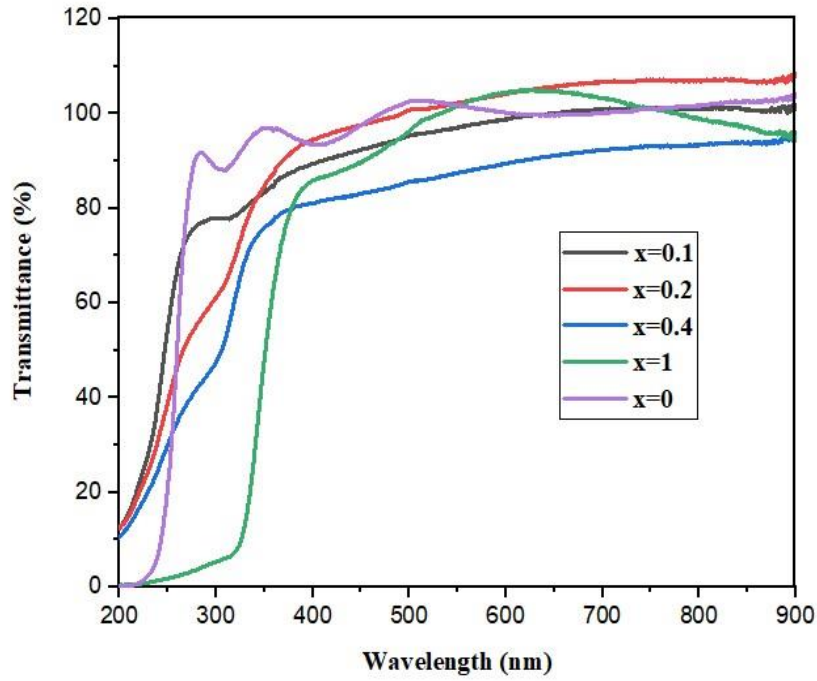
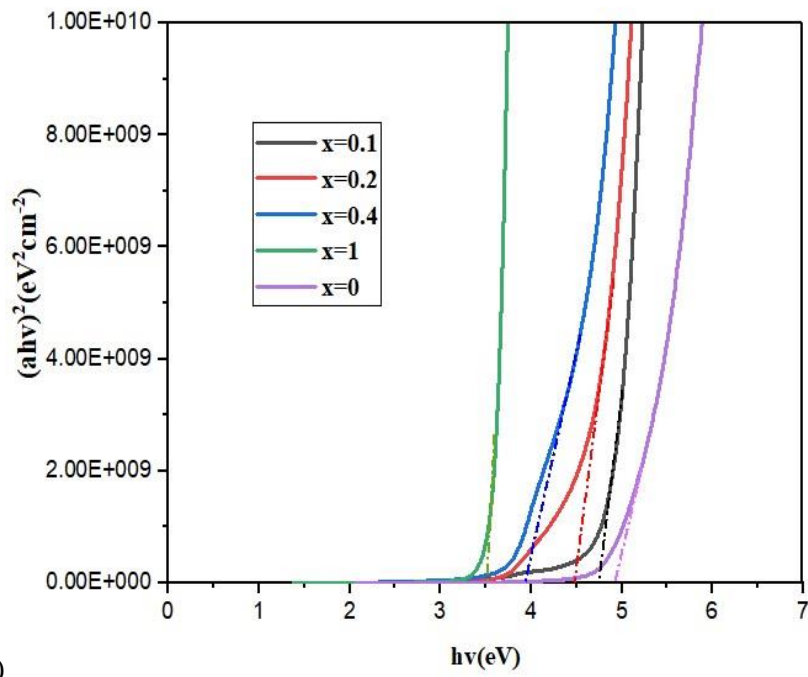


Figure 3.5: n and k (at $\lambda=632\text{nm}$) for $(\text{In}_x\text{Ga}_{1-x})_2\text{O}_3$ as a function of x

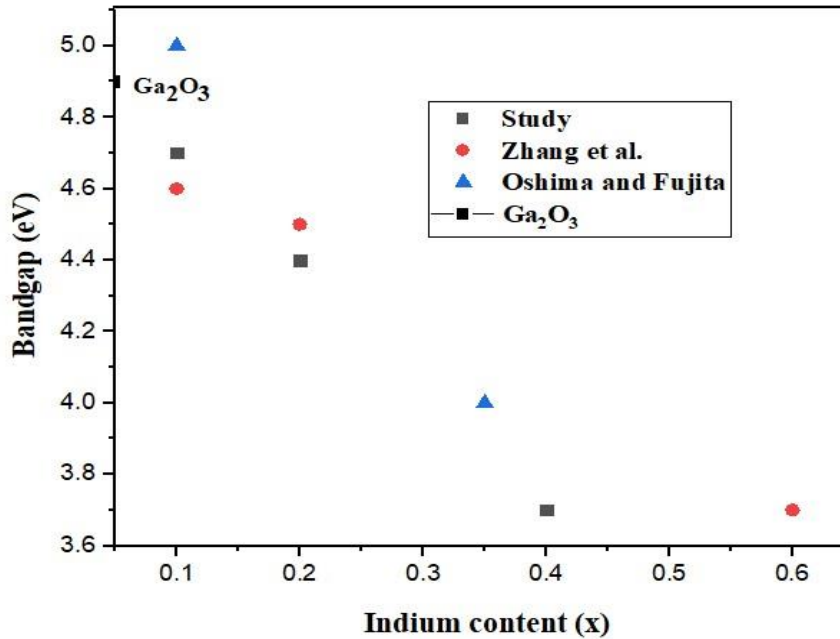
Ultraviolet-visible spectroscopy (UV-vis) measurements were taken for films with varying In content grown at a temperature of 650°C under an oxygen pressure of 10^{-2} Torr. Sharp absorption edges were clearly exhibited that shifted to a longer λ with increasing In content x as a result of a decrease in the bandgap. Transmittance was more than 80% in the visible range for all films as can be seen on figure 3.6 (a). Linear extrapolation of the plots to $h\nu=0$ was used to extract the optical bandgap of the films. The optical bandgap was found to decrease linearly with the increase in In content from 0.1 to 0.4 as shown in figure 3.6 (b). At the high absorption region, the linear relationships suggest a direct bandgap for the films. This is in accordance to previous research ^{[41][42]}. The optical bandgap values (E_g) have been plotted as a function of the In content x and has been compared to the values obtained in previous research ^{[41][42]} as shown in figure 3.6 (c). It is clear that the bandgap of films can be controlled by varying the indium content in the films leading to the fabrication of HEMT structures.



(a)



(b)



(c)

Figure 3.6: (a) Transmittance spectra (b) Tauc plot (c) Optical bandgap as a function of x compared to values obtained by previous literature; for samples varying in In content grown at temperature of 650°C and oxygen pressure 10^{-2} Torr.

Transmittance spectra was obtained for samples of In content $x=0.1$ grown at different temperatures 400°C and 650°C and oxygen pressure 10^{-2} Torr. The transmittance was > 80% in the visible region with a decrease in the transmissivity for the film grown at the higher substrate temperature as shown in figure 3.7. This could be due to a difference in the film thickness and/or surface morphology.

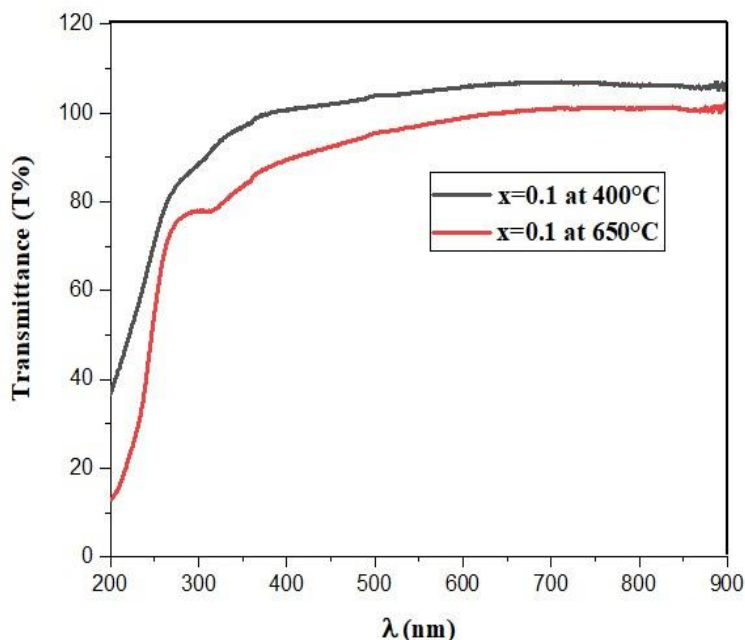
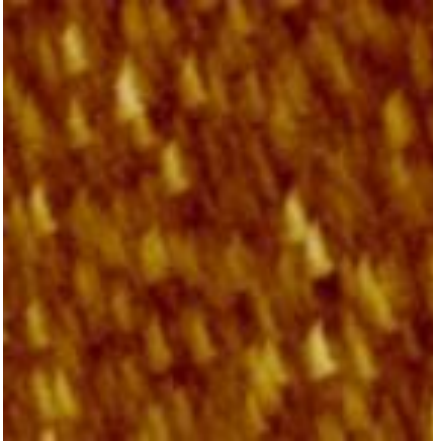


Figure 3.7: Transmittance spectra for samples of In content $x=0.1$, grown at different temperature and oxygen pressure of 10^{-2} Torr

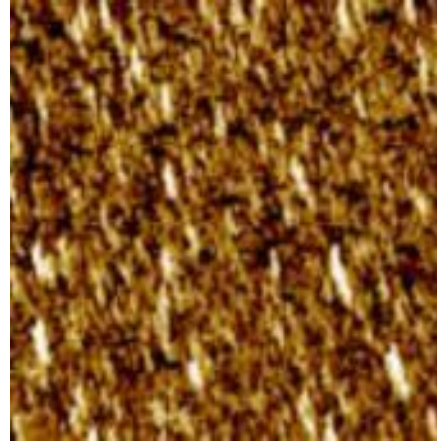
Atomic Force Microscopy (AFM) measurements were performed on samples having In content $x=0.2$ grown at a temperature of 650°C under different oxygen pressures as shown in figure 3.8, where P_{O_2} is the oxygen pressure during growth of the films. The surface roughness of film grown under oxygen pressure of 10^{-1} Torr was comparatively higher compared to the films grown at a lower pressure of 10^{-4} Torr. This could be explained by the decrease in grain size with lower oxygen pressure. Therefore, the oxygen pressure during growth of films played a role in determining the surface morphology of films.



Scale: $10 \times 10 \mu\text{m}^2$

$P_{\text{O}_2} = 10^{-1}$ Torr

roughness = 12 nm



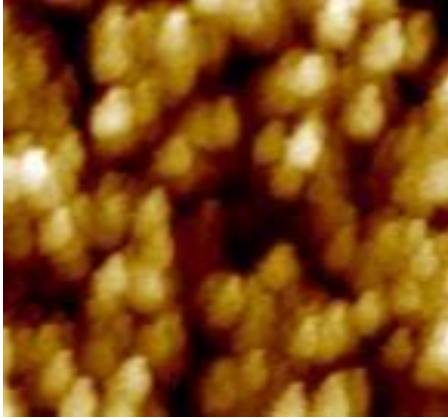
Scale: $10 \times 10 \mu\text{m}^2$

$P_{\text{O}_2} = 10^{-4}$ Torr

roughness = 1.8 nm

Figure 3.8: Atomic Force Microscopy (AFM) images of the films grown at a temperature of 650°C at different oxygen pressure

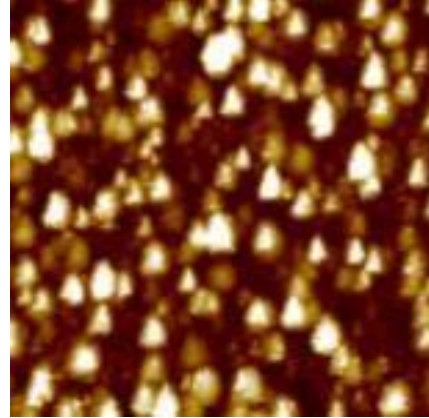
AFM images were taken for samples having indium content of 0.1, grown at the same oxygen pressure of 10^{-3} Torr but different substrate temperatures of 650°C and 700°C respectively as shown in figure 3.9. It was observed that the rms roughness of the sample grown at a higher temperature was greater than the sample grown at a lower temperature. This can be explained by the higher thermal energy generated to the ad-atoms to migrate on the surface of the sample grown at higher temperature. The crystallinity of the sample grown at higher temperature is greater because of increased nucleation.



Scale: $10 \times 10 \mu\text{m}^2$

$T_s = 650^\circ\text{C}$

roughness = 5 nm



Scale: $10 \times 10 \mu\text{m}^2$

$T_s = 700^\circ\text{C}$

roughness = 8 nm

Figure 3.9: AFM images of samples grown at 650°C and 700°C , at an oxygen pressure of 10^{-3} Torr.

IV. CONCLUSION

Films of $(\text{In}_x\text{Ga}_{1-x})_2\text{O}_3$ were grown by varying the In content from $x=0.1$ to $x=0.4$ at different substrate temperatures and oxygen pressures using pulsed laser deposition (PLD) technique. The effect of parameters such as composition of In (x), substrate temperature and oxygen pressure on the films were studied. X-ray diffraction (XRD) measurements revealed an increase in the lattice parameter as In content increased which could be explained by the high ionic radius of In compared to that of Ga. The films were found to exhibit polycrystalline cubic as well as monoclinic crystal structure at In content $x=0.1$ grown at 650°C . As the indium content increased from $x=0.1$ to $x=0.4$, the cubic structure of films was dominant. Spectroscopic Ellipsometry provided the optical properties of the films namely the refractive indices (n) and extinction coefficients (k). UV-Vis measurements helped in determining the optical bandgap of films. The optical bandgap was found to decrease with the increase in In content. Therefore, the optical bandgap of a material can be tuned by alloying. Atomic Force Microscopy (AFM) results revealed the surface morphology of films. In comparison to previous literature, this study reveals the optical and structural properties of grown films by varying growth parameters such as substrate temperature and oxygen pressure during growth.

REFERENCES

- [1] Josef Lutz, Heinrich Schlangenotto, Uwe Scheuermann, Rik De Doncker, *Semiconductor Power Devices: Physics, Characteristics, Reliability, Second Edition*. Springer International Publishing AG 2018
- [2] T. C. Lovejoy, *III-VI semiconductors and oxides: Electronic structure, surface morphology, and transition metal doping of gallium selenide, indium selenide, and gallium oxide*. 2010.
- [3] T.-C. Wei, D.-S. Tsai, P. Ravadgar, J.-J. Ke, M.-L. Tsai, D.-H. Lien, C.-Y. Huang, R.-H. Horng, and J.-H. He, "See-Through Ga₂O₃ Solar-Blind Photodetectors for Use in Harsh Environments," *IEEE J. Sel. Top. Quantum Electron.*, vol. 20, no. 6, pp. 112–117, 2014.
- [4] E. Monroy, F. Omnès, and F. Calle, "Wide-bandgap semiconductor ultraviolet photodetectors," *Semicond. Sci. Technol.*, vol. 18, no. 4, p. R33, 2003.
- [5] Gyan Prakash Pal, Anuj Kumar Shrivastav, "High Electron Mobility Transistor (HEMT)" *International Journal of Scientific Research Engineering & Technology (IJSRET) Volume 1 Issue1 pp 043-046 March 2012*
- [6] <https://en.wikipedia.org>
- [7] G. Giusti, "Deposition and characterisation of functional ITO thin films," Ph.D., University of Birmingham (United Kingdom), England, 2011.
- [8] José Millán, Philippe Godignon, Amador Pérez-Tomás, "Wide Band Gap Semiconductor Devices for Power Electronics," *AUTOMATIKA*; APR-JUN 2012, 53 2, p107-p116, 10p.

- [9] S. I. Stepanov, V. I. Nikolaev, V. E. Bougrov, and A. E. Romanov, "Gallium oxide: Properties and applications - A review," *Rev. Adv. Mater. Sci.*, vol. 44, no. 1, pp. 63–86, 2016.
- [10] T. Onuma, S. Fujioka, T. Yamaguchi, M. Higashiwaki, K. Sasaki, T. Masui, and T. Honda, "Correlation between blue luminescence intensity and resistivity in β -Ga₂O₃ single crystals," *Appl. Phys. Lett.*, vol. 103, no. 4, p. 41910, 2013.
- [11] N. Ueda, H. Hosono, R. Waseda, and H. Kawazoe, "Synthesis and control of conductivity of ultraviolet transmitting beta-Ga₂O₃ single crystals," *Appl. Phys. Lett.*, vol. 70, pp. 3561–3563, 1997.
- [12] J. B. Varley, J. R. Weber, A. Janotti, and C. G. Van de Walle, "Oxygen vacancies and donor impurities in β -Ga₂O₃," *Appl. Phys. Lett.*, vol. 97, p. 142106, 2010
- [13] Oliver Bierwagen, "Indium oxide—a transparent, wide-band gap semiconductor for (opto)electronic Applications," Paul-Drude-Institut für Festkörperelektronik, Hausvogteiplatz 5– 7, 10117 Berlin, Germany.
- [14] M. Higashiwaki, K. Sasaki, A. Kuramata, T. Masui, and S. Yamakoshi, "Development of gallium oxide power devices," *Phys. status solidi*, vol. 211, no. 1, pp. 21–26, 2014.
- [15] S. Ghose, M. S. Rahman, J. S. Rojas-Ramirez, M. Caro, R. Droopad, A. Arias, and N. Nedev, "Structural and optical properties of β -Ga₂O₃ thin films grown by plasma-assisted molecular beam epitaxy," *J. Vac. Sci. Technol. B, Nanotechnol. Microelectron. Mater. Process. Meas. Phenom.*, vol. 34, no. 2, p. 02L109, 2016.

- [16] M. Higashiwaki, K. Sasaki, A. Kuramata, T. Masui, and S. Yamakoshi, "Gallium oxide (Ga_2O_3) metal-semiconductor field-effect transistors on single-crystal β - Ga_2O_3 (010) substrates," *Appl. Phys. Lett.*, vol. 100, no. 1, p. 13504, 2012.
- [17] J R Bellingham, W A Phillips, C J Adkins, "Electrical and optical properties of amorphous indium oxide," *Journal of Physics: Condensed Matter*, Volume 2, Issue 28, pp. 6207-6221 (1990).
- [18] T. de Boer, M. F. Bekheet, A. Gurlo, R. Riedel, A. Moewes, "Band gap and electronic structure of cubic, rhombohedral, and orthorhombic In_2O_3 polymorphs: Experiment and theory," *Physical Review B*, Volume 93, Issue 15, id.155205, 2016.
- [19] D. Bruce Buchholz, Qing Ma, Diego Alducin, Arturo Ponce, Miguel Jose-Yacaman, Rabi Khanal, Julia E. Medvedeva, Robert P. H. Chang, "The Structure and Properties of Amorphous Indium Oxide."
- [20] Fabi Zhang, Katsuhiko Saito, Tooru Tanaka, Mitsuhiro Nishio, Qixin Guo, "Wide bandgap engineering of $(\text{GaIn})_2\text{O}_3$ films," Department of Electrical and Electronic Engineering, Synchrotron Light Application Center, Saga University, Saga 840-8502, Japan
- [21] J. Ahman, G. Svensson and J. Albertsson *Acta Crystallogr. Sect. C Cryst. Struct. Commun.* 52 (1996) 1336.
- [22] S. Geller, *J. Chem. Phys.* 33 (1960) 676
- [23] C. Janowitz, V. Scherer, M. Mohamed, A. Krapf, H. Dwelk, R. Manzke, Z. Galazka, R. Uecker, K. Irmischer and R. Fornari, "Experimental electronic structure of In_2O_3 and Ga_2O_3 ," *New J. Phys.* 13 (2011) 085014

- [24] C. Xirouchaki, G. Kiriakidis, T. F. Pedersen, and H. Fritzsche, *J. Appl. Phys.* 79, 9349 ~1996
- [25] Bender, M.; Katsarakis, N.; Gargaoudakis, E.; Hourdakis, E.; Douloufakis, E.; Cimalla, V.; Kiriakidis, “Dependence of the photoreduction and oxidation behavior of indium oxide films on substrate temperature and film thickness,” *Applied Physics*. 11/15/2001, Vol. 90 Issue 10, p5382. 6p.
- [26] Facchetti, T.J. Marks (Eds.), *Transparent Electronics From Synthesis to Applications*, John Wiley & Sons Ltd., United Kingdom, 2010.
- [27] H. Ohta, M. Orita, M. Hirano, H. Tanji, H. Kawazoe, H. Hosono, “Highly electrically conductive indium-tin-oxide thin films epitaxially grown on yttria-stabilized zirconia (100) by pulsed-laser deposition,” *Applied Physics Letters* 76 (2000) 2740.
- [28] Subramani Shanmugan, Devarajan Mutharasu and Ibrahim Kamarulazizi, “Rhombohedral In_2O_3 Thin Films Preparation from In Metal Film using Oxygen Plasma,” in 2012 10th IEEE International Conference on Semiconductor Electronics (ICSE), 2012, pp. 711–715.
- [29] N. Bellakhal, K. Draou and J.L. Brisset, “Electrochemical investigation of copper oxide films formed by oxygen plasma treatment,” *J. Appl. Electrochem.* vol. 27, pp. 414–421, 1997.
- [30] P. Luzeau, X.Z.Xu, M. Lagues, N.Hess, J.P. Contour, et. al., “Copper oxide thin film growth using an oxygen plasma source” *J. Vac. Sci. Technol.* vol. A8, pp. 3938–3940, 1990.

- [31] Khadijeh Shamsoddini and Hosein Eshghi, "Effect of Deposition Rate and Annealing on Physical Properties of In_2O_3 Thin Films Prepared by Spray Pyrolysis: Ultraviolet (UV) Photoconductivity Response," *Journal of Electronic Materials*, July 2017, Volume 46, Issue 7, pp 4649–4655
- [32] Matthew Zervos Demetra Tsokkou Maria Pervolaraki Andreas Othono, "Low Temperature Growth of In_2O_3 and InN Nanocrystals on $\text{Si}(111)$ via Chemical Vapour Deposition Based on the Sublimation of NH_4Cl in In ," *Nanoscale Research Letters*, June 2009, 4:491
- [33] R. K. Gupta, N. Mamidi, K. Ghosh, S. R. Mishra, P. K Kahol, "Growth and characterization of In_2O_3 thin films prepared by pulsed laser deposition," *JOURNAL OF OPTOELECTRONICS AND ADVANCED MATERIALS*; JUL 2007, 9 7, p2211-p2216, 6p.
- [34] Z.X. Mei, Y. Wang, X.L. Dua, Z.Q. Zenga, M.J. Yinga, H. Zhenga, J.F. Jiaa, Q.K. Xuea, Z. Zhang, "Growth of In_2O_3 single-crystalline film on sapphire (0001) substrate by molecular beam epitaxy," *In Journal of Crystal Growth* 2006 289(2):686-689
- [35] Susmita Ghose, Shafiqur Rahman, Liang Hong, Juan Salvador Rojas-Ramirez, Hanbyul Jin, Kibog Park, Robert Klie, and Ravi Droopad, "Growth and characterization of $\beta\text{-Ga}_2\text{O}_3$ thin films by molecular beam epitaxy for deep-UV photodetectors," *J. Appl. Phys.* 122, 095302 (2017); <https://doi.org/10.1063/1.4985855>

- [36] Kohei Sasaki, Masataka Higashiwaki, Akito Kuramata, Takekazu Masui, Shigenobu Yamakoshi, "MBE grown Ga₂O₃ and its power device applications," In *The 17th International Conference on Molecular Beam Epitaxy*, Journal of Crystal Growth 1 September 2013 378:591-595
- [37] L. X. Qian, Y. Wang, Z. H. Wu, T. Sheng, and X. Z. Liu, "β-Ga₂O₃ solar-blind deep-ultraviolet photodetector based on annealed sapphire substrate," *Vacuum*, vol. 140, no. Supplement C, pp. 106–110, Jun. 2017.
- [38] P. Marie, X. Portier, and J. Cardin, "Growth and characterization of gallium oxide thin films by radiofrequency magnetron sputtering," In: *Physica Status Solidi (A) Applications and Materials Science*. (Physica Status Solidi (A) Applications and Materials Science, August 2008, 205(8):1943-1946)
- [39] T. Minami, Y. Takeda, T. Kakumu, S. Takata, and I. Fukuda, "Preparation of highly transparent and conducting Ga₂O₃–In₂O₃ films by direct current magnetron sputtering," *J. Vac. Sci. Technol. A Vacuum, Surfaces, Film.*, vol. 15, no. 3, pp. 958–962, 1997.
- [40] J. M. Phillips, J. Kwo, G. A. Thomas, S. A. Carter, R. J. Cava, S. Y. Hou, J. J. Krajewski, J. H. Marshall, W. F. Peck, and D. H. Rapkine, "Transparent conducting thin films of GaInO₃," *Appl. Phys. Lett.*, vol. 65, no. 1, pp. 115–117, 1994.

- [41] Takayoshi Oshima, and Shizuo Fujita, "Properties of Ga_2O_3 -based $(\text{In}_x\text{Ga}_{1-x})_2\text{O}_3$ alloy thin films grown by molecular beam epitaxy," In: *Physica Status Solidi (C) Current Topics in Solid State Physics, Papers Presented at the 34th International Symposium on Compound Semiconductors, ISCS-2007*. (*Physica Status Solidi (C) Current Topics in Solid State Physics*, 2008, 5(9):3113-3115)
- [42] H. von Wenckstern et al., "Structural and optical properties of $(\text{InGa})_2\text{O}_3$ thin films and characteristics of Schottky contacts thereon," *Semicond. Sci. Technol.*, vol. 30, no. 2, p. 024005, 2015.
- [43] Fabi Zhang, Hideki Jan, Katsuhiko Saito, Tooru Tanaka, Mitsuhiro Nishio, Takashi Nagaoka, Makoto Arita, Qixin Guo, "Toward the understanding of annealing effects on $(\text{GaIn})_2\text{O}_3$ films," In *Thin Solid Films* 2 March 2015 578:1-6
- [44] Doreen D. Edwards, Pollyanna E. Folkins, and Thomas O. Mason, "Phase Equilibria in the Ga_2O_3 - In_2O_3 System," *Journal of the American Ceramic Society*, Jan 1997.
- [45] J. Chang, Y. L. Zhou, Y. Zhou, "Bioactive Glasses, 2- Surface modification of bioactive glasses," *Materials, Properties and Applications*, Woodhead Publishing Series in Biomaterials, 2011.
- [46] A. Sarangan, "Fundamentals and Applications of Nanophotonics: Nanofabrication,"
- [47] J. Pou, F. Lusquiños, R. Comesaña, M. Boutinguiza, "Advances in Laser Materials Processing, 14- Production of biomaterial coatings by laser-assisted processes," *Technology, Research and Application*, Woodhead Publishing Series in Welding and Other Joining Technologies, 2010.

- [48] A. K. Chatterjee, "X-Ray Diffraction," Handbook of Analytical Techniques in Concrete Science and Technology, 2001.
- [49] Handbook of Silicon Based MEMS Materials and Technologies (Second Edition); Chapter 15 - Silicon Wafer and Thin Film Measurements; 2015.
- [50] H. G. Tompkins, E. A. Irene, and ScienceDirect Freedom (Patron driven), Eds., Handbook of ellipsometry. Norwich, NY : Heidelberg, Germany: William Andrew Pub. ; Springer, 2005.
- [51] H.-H. Perkampus, UV-VIS Spectroscopy and Its Applications. Berlin Heidelberg;; Springer-Verlag, 1992.
- [52] R. Waser, *Nanoelectronics and information technology*. John Wiley & Sons, 2012.
- [53] Y. Yan; 7-Metals for Biomedical Devices, Woodhead Publishing Series in Biomaterials, 2010.
- [54] S. Morita, F. J. Giessibl, E. Meyer, and R. Wiesendanger, *Noncontact atomic force microscopy*, vol. 3. Springer, 2015.
- [55] G. Binnig, C. F. Quate, and C. Gerber, "Atomic force microscope," *Phys. Rev. Lett.*, vol. 56, no. 9, p. 930, 1986.
- [56] F. J. Giessibl, "Advances in atomic force microscopy," *Rev. Mod. Phys.*, vol. 75, no. 3, p. 949, 2003.
- [57] G. M. McClelland, R. Erlandsson, and S. Chiang, "Atomic force microscopy: General principles and a new implementation," in *Review of Progress in Quantitative Nondestructive Evaluation*, Springer, 1987, pp. 1307–1314.